# Protein kinase CK2 alpha prime and alpha-synuclein constitute a key regulatory pathway in Huntington's disease

Dahyun Yu[1,5], Nicole Zarate[1,5], Francesco Cuccu[1,3], Johnny S. Yue, Taylor G. Brown[1], Adelyn Tsai[1], Rachel Mansky[1], Kevin Jiang[1], Hyuck Kim[1#], Carmen Nanclares[1], Tessa Nichols-Meade[1], Sarah N. Larson[2], Katie Gundry[2], Ying Zhang[4], Michael Benneyworth[1], Gülin Öz[2], Marija Cvetanovic[1], Alfonso Araque[1] and Rocio Gomez-Pastor[1±].

[1]Department of Neuroscience, School of Medicine, University of Minnesota, Minneapolis, MN, United States. [2]Center for Magnetic Resonance Research. Department of Radiology, School of Medicine, University of Minnesota, Minneapolis, MN, United States. [3]Department of Life and Environment Sciences, University of Cagliari, Cagliari, Italy. [4] Minnesota supercomputing Institute, University of Minnesota. Minneapolis, MN, United States

#Current address: Department of Neuroscience, Institute for Inflammation Control Korea University College of Medicine, Seoul, South Korea

[5]These authors contributed equally to the manuscript.

± Correspondence should be addressed to Rocio Gomez-Pastor, University of Minnesota, 321 Church St. SE, Jackson Hall Room 6-145, Minneapolis, MN 55455, rgomezpa@umn.edu

## Summary

Huntington's Disease (HD) is a neurodegenerative disorder caused by a polyglutamine expansion in the HTT protein. This mutation causes HTT misfolding and aggregation, preferentially affecting neurons of the basal ganglia. Other aggregation-prone proteins like alpha-synuclein (α-syn), mostly associated with Parkinson's disease (PD), has recently been involved in motor deficits in HD, but its mechanism of action is unknown. Here we showed that α-syn serine 129 phosphorylation (α-syn-pS129), a posttranslational modification linked to α-synucleinopathy, is highly phosphorylated in the brain of symptomatic zQ175 HD mice. We demonstrated that such phosphorylation is mediated by Protein Kinase CK2 alpha prime (CK2α'), which is preferentially induced in striatal neurons in HD. Knocking out one allele of CK2α' in zQ175 mice decreased α-syn-pS129 in the striatum and ameliorated several HD-like symptoms including neuroinflammation, transcriptional alterations, excitatory synaptic transmission deficits and motor dysfunction. Our data suggests CK2α'-mediated synucleinopathy as a key molecular mechanism of neurodegeneration in HD.

## Introduction

Huntington's disease (HD) is a neurodegenerative disorder that manifests with progressive motor, cognitive, and psychiatric deficits for which there is no cure. HD is caused by a poly-glutamine (polyQ) expansion in exon1 of the Huntingtin (*HTT*) gene. This mutation results in progressive misfolding and aggregation of mutant HTT protein (mHTT) and preferentially affects GABAergic medium spiny neurons (MSNs) in the striatum (1993, DiFiglia et al. 1997, Ferrante, Kowall, and Richardson 1991). Transcriptional perturbations in synaptic genes and neuroinflammation are key processes that precede MSN death and motor symptom onset (Crotti and Glass 2015). However, our understanding of the interplay between these processes, mHTT aggregation and their contribution to MSN susceptibility in HD is still incomplete.

Neuroinflammation is a complex combination of responses between neurons and glial cells (microglia and astrocytes). mHTT induces several pro-inflammatory cytokines such as interleukins IL-1β and IL6, tumor necrosis factor TNF-α, and other neurotoxic molecules that contribute to propagating damage across the brain (Crotti and Glass 2015). These cytokines alter cell-cell interactions and impair neuronal transcription, neurotransmitter regulation, $Ca^{2+}$ homeostasis and G-protein coupled receptor functions, ultimately leading to neuronal dysfunction and death (Turner et al. 2014). Increased pro-inflammatory cytokines can also modulate astrocytic proliferation and their transcriptional landscape (Clarke et al. 2018, Liddelow et al. 2017). Diaz-Castro et al. showed that HD astrocytes present a unique transcriptional signature representative of astrocytic dysfunction and such deficits contribute to MSN death. Astrocytes play a fundamental role in the regulation of neuronal function and synaptic plasticity (Eroglu

and Barres 2010, Araque et al. 1999) and conditional mHTT KO in astrocytes of BACHD mice rescued levels of synaptic proteins, increased MSN excitability and improved motor behavior (Wood et al. 2019). Astrocytic dysfunction has been well documented in HD and is an important contributor to the onset and progression of HD symptoms in mice (Khakh et al. 2017). Therefore, developing pharmacological strategies to improve astrocyte health in HD and other neurodegenerative diseases (NDs) is of great interest.

Protein kinase CK2 is at the crossroads between neuroinflammation, glial function and synaptic activity and has recently emerged as a potential therapeutic target in neurodegeneration (Castello et al. 2017). Pharmacological inhibition of CK2 in cell cultures expressing amyloid beta (Aβ) reduced Aβ aggregation and the production of pro-inflammatory cytokines and increased cell viability (Rosenberger et al. 2016). In neural stem cells from neonatal mice, CK2 inhibition also modulated gliogenesis (Bender et al. 2017). CK2 is a highly conserved serine/threonine kinase composed of two regulatory beta (CK2β) and two catalytic subunits, alpha (CK2α) and alpha prime (CK2α') (Niefind et al. 2001, Olsen et al. 2006, Pinna 2002, Litchfield 2003). The two catalytic subunits share high structural homology, but they differ in their tissue distribution and their ability to phosphorylate different substrates (Xu et al. 1999, Litchfield 2003, Bian et al. 2013, Ceglia, Flajolet, and Rebholz 2011). Our previous work showed that CK2α', but not CK2α, is induced in HD MSNs and is responsible for the phosphorylation and degradation of the heat shock transcription factor HSF1, the master regulator of chaperones and protein quality control systems (Gomez-Pastor et al. 2017, Gomez-Pastor, Burchfiel, and Thiele 2017). CK2α'-dependent degradation of

HSF1 contributes to chaperones dysregulation and HTT aggregation in cells and mouse models of HD (Gomez-Pastor et al. 2017). However, other studies conducted *in vitro* have suggested a protective role of CK2 in HD (Fan et al. 2008a, Atwal et al. 2011) imposing the necessity to clarify the specific involvement of CK2α' in HD pathogenesis and its potential as a therapeutic target in HD.

In addition, CK2 has been involved in the phosphorylation and induced aggregation of other pathological proteins like MAPT (microtubule associated protein tau) and alpha-synuclein (α-syn), proteins involved in Alzheimer's (AD) and Parkinson's disease (PD) (Greenwood et al. 1994, Masliah et al. 1992, Takahashi et al. 2007, Waxman and Giasson 2008, 2011). Interestingly, tau and α-syn also seem to contribute to HD pathology (Tomás-Zapico et al. 2012, Fernández-Nogales et al. 2014). Specific tau modifications and cleavage products associated with cognitive decline in AD were found in the brains of HD patients and suggested HD as a new tauopathy (Liu et al. 2020, Fernández-Nogales et al. 2014). Similarly, increased levels of α-syn were observed in plasma of patients with HD (Shalash et al. 2017, Breza et al. 2020). α-syn was colocalized with mHTT aggregates in the brain of R6/1 HD mice, and its deletion resulted in amelioration of motor deficits (Tomás-Zapico et al. 2012). Tau and α-syn were related to neuroinflammatory processes, transcriptional dysregulation and synaptic deficits in AD and PD (Hoenen et al. 2016, Ising et al. 2019, Masliah et al. 2000, Zach et al. 2007), all of which are also seen in HD. However, the mechanisms by which these proteins are altered in HD and the extent to which they contribute to HD pathophysiology is still unknown.

In this study we characterized the role of CK2α' in HD *in vivo* by using the heterozygous zQ175 HD mouse model lacking one allele of CK2α'. We showed that CK2α' haploinsufficiency decreased the levels of pro-inflammatory cytokines and improved astrocyte health, restored synaptic gene expression and excitatory synapse function, and improved motor behavior in zQ175 mice. We also demonstrated that neuropathological and phenotypic changes in HD mice correlated with an increase in α-syn Ser129 phosphorylation in the striatum, a posttranslational modification involved in α-syn pathology in PD. Depletion of CK2α' decreased α-syn-pS129, establishing a novel connection between CK2α' function and synucleinopathy in HD. Collectively, our data demonstrated that CK2α' plays a negative role in HD and points to the potential of modulating CK2α' to achieve enhanced neuronal function and neuroprotection.

## Results

### Increased CK2α' levels in the striatum of zQ175 mice parallel progressive HTT aggregation and neuronal loss

Increased protein kinase CK2 activity has been associated with detrimental effects in protein homeostasis and neuroinflammation in different neurodegenerative diseases (Castello et al. 2017) but its role in HD is still controversial (Gomez-Pastor et al. 2017, Atwal et al. 2011, Fan et al. 2008b). To determine whether CK2α' plays a negative role during HD pathogenesis we first evaluated the relationship between HTT aggregation, neuronal loss and CK2α' level over time in the striatum of the heterozygous zQ175 mouse model (Menalled et al. 2012b). This knock-in mouse model has the

mouse *Htt* exon 1 replaced by the human *HTT* exon 1 sequence with a ~190 CAG repeat tract in the C57BL/6J background. Heterozygous zQ175 mice show motor deficits from around 4.5 months of age, followed by motivational deficits at 6 months of age and learning deficits at around 12 months of age (Heikkinen et al. 2012, Menalled et al. 2012b). We studied mice at 3 months (pre-symptomatic), 6 months (early symptomatic), 12 months (symptomatic) and 22 months (late stage disease). We observed a significant increase of HTT aggregates in the striatum, as evaluated by the levels of EM48 signal, in HD mice starting at 6 months of age and increasing in an age-dependent manner (**Fig. 1A, B**). In contrast, the number of neurons, using the neuronal marker NeuN, showed a significant decrease over time starting at 12 months (**Fig. 1C, D, S1A**). We confirmed that the loss of NeuN+ cells correlated with the specific loss of MSNs, using the MSN marker Ctip2 (Arlotta et al. 2008) (**Fig. S1B, C**). When comparing the timing of HTT aggregation and neuronal loss, we found the loss of neurons to be delayed compared to the appearance of aggregates (**Fig. 1B, D**). The levels of CK2α' in the striatum increased over time starting at 6 months (**Fig. 1E, F**), coinciding with the time at which we observed a significant increase in HTT aggregation (**Fig. 1A**) and preceding the onset of neuronal loss at 12 months. The accumulation of CK2α' in HD was restricted to the striatum, as previously reported (Gomez-Pastor et al. 2017), with no upregulation observed in the cortex (**Fig. 1G**). Regression analysis demonstrated that CK2α' levels had a significant positive relationship with HTT aggregation (Pearson $r(22)=0.87$, p value<0.001) (**Fig. 1H**) and a significant negative relationship with neuronal number (Pearson $r(22)=-0.78$, p value<0.001) (**Fig. 1I**).

## CK2α' haploinsufficiency reduced production of inflammatory cytokines in zQ175 mice without altering microglia

CK2 is known to regulate transcription factors, aggregation-prone proteins and signaling pathways involved in inflammation (Singh and Ramji 2008). Therefore, the accumulation of CK2α' in the striatum of HD mice and patients (Gomez-Pastor et al. 2017, Fan et al. 2008a) could be related to the activation of neuroinflammatory processes. HTT aggregates as well as components of dead neurons can trigger the activation of inflammatory processes in the brain, leading to the accumulation of pro-inflammatory cytokines (i.e. IL-6 and TNF-α) that amplify inflammatory signals and result in increased neurotoxicity (Crotti and Glass 2015, Luthi-Carter et al. 2000, Pido-Lopez et al. 2019, Reinhart et al. 2011). Accumulation of IL-6 in plasma and cerebrospinal fluid (CSF) from patients with HD is used as a marker of disease progression (Björkqvist et al. 2008, Chang et al. 2015). To determine whether the expression of CK2α' is directly related to neuronal-mediated inflammation in HD, we analyzed the levels of IL-6 in the striatal-derived mouse cells ST*Hdh*$^{Q7/Q7}$ (control) and ST*Hdh*$^{Q111/Q111}$ (HD cells) (**Fig. 2A**). RT-qPCR analysis showed upregulation of CK2α' in HD cells paralleled the upregulation of IL-6. We then silenced the expression of CK2α' using siRNA in HD cells (**Fig. 2B**). Reduced mRNA levels of IL-6 were observed with CK2α' silencing when compared to non-targeting siRNA (scramble). These data suggested a potential connection between the neuronal upregulation of CK2α' and increased expression of pro-inflammatory cytokines in HD.

To further explore the role of CK2α' in modulating inflammation in HD, we used the zQ175 mouse model lacking one allele of CK2α' (zQ175:CK2α'$^{(+/-)}$), previously

generated in our lab (Gomez-Pastor et al. 2017) (**Fig. 2C**). CK2α' homozygous KO mice are viable but present with globozoospermia, male sterility, and difficult breeding (Xu et al. 1999). Therefore, we focused our experiments on the CK2α' heterozygous KO which do not present phenotypic differences compared to WT mice and have previously shown positive effects in reducing HTT aggregation when crossbred with HD mice (Gomez-Pastor et al. 2017). We showed that zQ175:CK2α'$^{(+/-)}$ resulted in approximately 50% reduction of CK2α' levels in MSNs (Ctip2+ CK2α'+ cells) compared to zQ175 mice (**Fig. 2D**). The levels of 40 different cytokines and chemokines were analyzed in protein extracts obtained from the striatum of WT, zQ175 and zQ175:CK2α'$^{(+/-)}$ mice at symptomatic age (12-14 months) using the mouse cytokines proteome profiling array (R&D systems ARY006) (n=6 mice/genotype with a female(F)/male(M) ratio: 3F/3M WT, 5F/1M zQ175 and 4F/2M zQ175:CK2α'$^{(+/-)}$) (**Fig. 2E, S2A-D**). The relative levels of eleven pro-inflammatory cytokines, including GM-CSF, IFN-γ, IL-1α, IL-1β, IL-1ra, IL-7, IL-16, IL-17, IL-23, IL-27, and TNF-α, were significantly higher in extracts from HD mice compared with WT (**Fig. 2F**). Of the eleven induced cytokines, IFN-γ, IL-1α, IL-16, and TNF-α showed much greater relative levels of expression than the rest. No significant differences were observed in the amount of several analyzed chemokines (**Fig. S2B, D**). Surprisingly, zQ175:CK2α'$^{(+/-)}$ mice showed significantly lower levels of seven cytokines (IFN-γ, IL-1α, IL-7, IL-16, IL-17, IL-23, and TNF-α) than those in zQ175 mice (**Fig. 2F**). Decreased levels of IL-6 were also found in zQ175:CK2α'$^{(+/-)}$ mice, albeit its levels were not induced in the striatum of zQ175 mice at the time point analyzed. Collectively, these data indicate that CK2α' directly or indirectly contributes to the expression of various cytokines in the striatum during HD and suggest that the

characteristic inflammatory profile of HD could be triggered in a CK2α'-dependent manner.

The accumulation of pro-inflammatory cytokines, other inflammatory mediators, and molecules secreted from damaged neurons often result in the activation of microglia, the resident macrophages of the central nervous system (CNS) that respond to degenerated neurons and facilitate immunomodulatory and phagocytic activities. Activation of microglia, which is characterized by swollen shapes and the retraction of processes, has been observed using positron emission tomography (PET) in pre-symptomatic patients with HD and reported in numerous HD mouse models (Pavese et al. 2006, Tai et al. 2007, Savage et al. 2020). There is mounting evidence that microglia play an important role in HD pathogenesis, but the extent of their contribution and the exact timing at which activated microglia are essential in HD is still under debate. To determine whether changes in the production of pro-inflammatory cytokines in zQ175:CK2α'$^{(+/-)}$ mice are caused by alterations in the activation of microglia, we first evaluated the total levels of the microglial marker Iba1 (Ionized calcium binding adaptor molecule 1) by immunoblotting (IB) in striatum extracts from WT, zQ175, and zQ175:CK2α'$^{(+/-)}$ mice at 12-14 months of age, an age where the proinflammatory cytokines were induced (**Fig. S3A, B**). We observed that total Iba1 levels were significantly increased in zQ715 and zQ175:CK2α'$^{(+/-)}$ mice compared to WT, indicative of microgliosis, but no significant differences were observed between zQ175 and zQ175:CK2α'$^{(+/-)}$ mice. However, when the number and area size of microglial cells were evaluated by Iba1 immunofluorescence (IF) analyses, only a non-significant trend towards increased microgliosis was seen in the HD mice (**Fig. 3G-I**). We do not have a

good explanation to reconcile our Iba1 IB and IF data other than our IB data may be capturing all the Iba1 present in microglial processes while our IF data only counts Iba1+ cell bodies. Nevertheless, our IF data are consistent with recent reports using Iba1 IF in zQ175 mice at this same age that also reported the absence of significant microgliosis (Diaz-Castro et al. 2019). Similar results were obtained in the R6/2 mice where an increased number of Iba1+ cell bodies as well as Iba1+ body area using IF were only significant at pre-symptomatic stages (Savage et al. 2020). Therefore, although microglia may play an important role during early HD pathogenesis, their role could become less relevant at later stages of the disease. All together our data suggested that CK2α'-mediated changes in the levels of pro-inflammatory cytokines in symptomatic zQ175:CK2α'$^{(+/-)}$ mice is not related to changes in activated microglia.

**CK2α' contributes to astrocyte pathology in HD**

In addition to microglia, astrocytes are also glial cells that can respond to pathological changes by releasing inflammatory factors and cytotoxins through reactive astrogliosis. Reactive astrocytes are characterized by molecular, cellular, and functional changes including hypertrophy of the soma and processes as well as increased proliferation (Anderson, Ao, and Sofroniew 2014). Increases in the number of astrocytes and astrocytic dysfunction is reported in several neurodegenerative diseases (Li et al. 2019), including HD (Diaz-Castro et al. 2019, Garcia et al. 2019, Khakh et al. 2017). Therefore, we tested whether the changes in CK2α' expression and cytokine levels were related to changes in astrocyte proliferation and dysfunction during HD pathogenesis. We

quantified the number of anti-glutamine synthetase (GS, astrocyte marker) immunoreactive cells (GS+) in the striatum of brain sections from 6, 12, and 22 month-old mice of WT, zQ175, and zQ175:CK2α'$^{(+/-)}$. zQ175 mice displayed a significant increase in the number of GS+ astrocytes over time compared to WT mice with the greatest difference observed at 12 months of age (**Fig. 3A, B**). Interestingly, although CK2α' expression is restricted to MSNs, as observed by the lack of colocalization between CK2α' and GS (**Fig. 3A**), CK2α' haploinsufficiency resulted in a significant decrease in the number of GS+ cells at all tested ages (**Fig. 3B**). At 22 months we observed significantly higher number of astrocytes in zQ175:CK2α'$^{(+/-)}$ mice compared with WT but it was still significantly lower than HD mice (**Fig. 3B**). To confirm that the changes indicating astrogliosis were not due to postmortem changes in brain slices, we performed proton magnetic resonance spectroscopy ($^{1}$H-MRS) *in vivo* at 22 months and measured the concentration of 15 different brain metabolites (**Fig. 3C, D, S4A, B**). The concentration of different neuronal metabolites including N-acetylaspartate (NAA) and glutamate, which are dysregulated in HD (Tkac et al. 2012, Peng et al. 2016, Heikkinen et al. 2012), did not differ between zQ175 and zQ175:CK2α'$^{(+/-)}$ mice (**Fig. S4A, B**). However, the levels of *myo*-inositol (Ins), widely considered an astroglial marker for its high abundance in astrocytic membranes (Castillo et al. 1998, Brand, Richter-Landsberg, and Leibfritz 1993), showed a significant reduction in zQ175:CK2α'$^{(+/-)}$ compared to zQ175 mice, although both the zQ175:CK2α'$^{(+/-)}$ and zQ175 mice had significantly higher mIns levels than WT mice (**Fig. 3D**). Despite seeing significant differences in the number of astrocytes between the three genotypes, no significant differences were observed in the striatum volume (**Fig. S4C, D**). Taken together, these

data suggested that increased CK2α' levels in HD MSNs may contribute to striatal astrogliosis.

Recent reports indicate that released cytokines like IL-1α, TNF-α, and complement component 1q (C1q) have the ability to induce specific transcriptional changes in astrocytes that allow them to acquire neuroinflammatory and cytotoxic functions (so called A1 astrocytes) (Liddelow et al. 2017, Clarke et al. 2018). The presence of these A1 astrocytes appears to be enhanced during aging and in different neurodegenerative diseases (Liddelow et al. 2017, Clarke et al. 2018), although their role in neuronal death in vivo is still unknown. A1 astrocytes are characterized by specific transcriptional changes and the accumulation of the complement component C3d protein (Liddelow et al. 2017, Clarke et al. 2018), a protein involved in innate immunity. While the presence of A1 astrocytic transcriptional signatures in HD has been refuted (Al-Dalahmah et al. 2020, Diaz-Castro et al. 2019), there seems to be consensus that increased depositions of C3d in astrocytes can be considered a marker of astrocyte pathology (Singhrao et al. 1999, Liddelow et al. 2017, Diaz-Castro et al. 2019). Since IL-1α and TNF-α are both induced in HD mice, and depletion of CK2α' decreased their expression, we evaluated whether CK2α' depletion could also impact astrocytes' health by altering the levels of C3d in astrocytes.

We first performed IF analyses for C3d in the striatum of WT, zQ175, and zQ175:CK2α'$^{(+/-)}$ mice at different ages and quantified the total intensity of C3d signal x area (**Fig. 3E, F**). These data revealed a significant age-dependent increase in the intensity of C3d in zQ175 mice compared to WT mice, which was more evident at 12 and 22 months of age. Similarly, zQ175:CK2α'$^{(+/-)}$ mice also showed an age-dependent

increase in the total levels of C3d compared to WT but these were significantly lower than in zQ175 mice (**Fig. 3F**).These data are consistent with previous reports indicating increased depositions of C3d in the striatum of HD patients (Liddelow et al. 2017, Singhrao et al. 1999). However, since increased C3d signal could be related to different striatal components other than astrocytes, such as neurons and myelin (Singhrao et al. 1999), these data cannot be directly associated with the health of astrocytes. Therefore, we next determined the fraction of GS+ astrocytes that showed C3d deposition (GS+C3d+ immunoreactive astrocytes) (**Fig. 3E, E', G**). Similar to total C3d levels, we observed an age-dependent increase in the percentage of GS+C3d+ astrocytes for all genotypes including WT mice. The levels of C3d in HD mice were significantly higher than WT mice at all time points analyzed (**Fig. 3G**). This increase in GS+C3d+ astrocytes in HD coincides with an increase in the accumulation of CK2α' in MSNs (**Fig. 1C**) and precedes neuronal death (**Fig. 1B**). In contrast, GS+C3d+ astrocyte data showed a significant reduction in zQ175:CK2α'$^{(+/-)}$ mice compared to zQ175 mice at 12 and 22 months and no significant differences between zQ175:CK2α'$^{(+/-)}$ and WT mice at any time point (**Fig. 3G**). Overall, these results suggest that neuronal accumulation of CK2α' could contribute to astrocyte proliferation and astrocyte pathology in HD.

## Depletion of CK2α' improves neuronal function and motor behavior

Recent transcriptional analyses in astrocytes from patients with HD and different HD mouse models revealed a specific transcriptional signature consistent with progressive loss of essential neuronal functions including calcium-dependent processes,

neurotransmitter regulation, and glutamate receptor signaling (Diaz-Castro et al. 2019, Al-Dalahmah et al. 2020). These functions are intimately related to the regulation of neuronal activity and synaptic plasticity (Araque et al. 1999). Perturbations in electrophysiological properties of MSNs have been widely reported in various HD mouse models (Zeron et al. 2002, Milnerwood and Raymond 2010, Kolodziejczyk and Raymond 2016). Early loss of thalamo-striatal signaling is followed by progressive deterioration of cortico-striatal input, resulting in overall decreased excitatory synaptic transmission in the HD striatum (Kolodziejczyk and Raymond 2016, Deng et al. 2014), contributing to the behavioral deficits associated with HD. Conditional mutant HTT knock-out in astrocytes improved astrocyte function and restored both synaptic protein expression and MSN excitability in the BACHD mouse model, demonstrating the intimate relationship between astrocyte health and synaptic function (Wood et al. 2019).

We assessed the impact of CK2α' depletion in AMPA-mediated excitatory transmission to determine whether improved health of astrocytes correlated with increased synaptic function. Whole-cell patch clamp recordings were obtained from acute dorsolateral striatum coronal slices from WT, zQ175, and zQ175:CK2α'$^{(+/-)}$ mice at 12 months old (**Fig. 4A**). MSNs from all genotypes showed similar profiles in the analysis of basal synaptic transmission, including input/output curves, paired-pulse facilitation, and synaptic fatigue (**Fig. 4B-D**). When we examined spontaneous neurotransmitter release and synaptic activity via recording of miniature excitatory postsynaptic currents (mEPSCs), we found that mEPSC amplitude, reflecting postsynaptic AMPA receptor function, was comparable among the 3 genotypes (**Fig. 4E**). However, mEPSC

frequency, which reflects the probability of neurotransmitter release from presynaptic vesicles and is also correlated to the number of synapses, was reduced in zQ175 mice (**Fig. 4F, G**), as previously reported (Indersmitten et al. 2015). Interestingly, this impairment in neurotransmission was reversed in the zQ175:CK2α'$^{(+/-)}$ mice, suggesting an improvement in presynaptic vesicular release. We observed that CK2α' haploinsufficiency did not affect the number of MSNs (Ctip2+ cells) or the mRNA levels of the MSN markers Drd1 (dopamine receptor 1, marker of MSNs of the direct pathway) and Drd2 (dopamine receptor 2, marker of MSNs of the indirect pathway) in the striatum compared to HD mice (**Fig. S5A-B**). Therefore, increased mEPSC frequency in zQ175:CK2α'$^{(+/-)}$ mice cannot be attributed to a greater number of neurons within the striatum. However, we observed significant increases in the levels of synaptic proteins like the scaffold protein Dlg4 (PSD-95), and Ppp1rb1 (dopamine- and cAMP-regulated neuronal phosphoprotein DARPP-32), a key regulator of the electrophysiological responses in striatal neurons (Fienberg et al. 1998, Vezzoli et al. 2019) (**Fig. S5C**). Similar results in levels of these synaptic proteins have been seen in neurons from BACHD mice lacking mHTT in astrocytes (Wood et al. 2019), indicating that astrocyte health can influence neuronal synaptic protein levels and excitability.

Improved strength of glutamatergic synaptic transmission is often related to improved motor control and cognitive processes in HD mouse models (Smith-Dijak, Sepers, and Raymond 2019, Vezzoli et al. 2019). To assess the impact of CK2α' haploinsufficiency on motor function, we conducted a series of motor tests including accelerating rotarod and beam walk comparing 3-month (pre-symptomatic) and 12-month-old (symptomatic) mice (**Fig. 5**). We also conducted cylinder and open field assessments exclusively in

12-month-old mice comparing zQ175 and zQ175:CK2α'$^{(+/-)}$ (**Fig. S6A-F**). The accelerating rotarod test did not show significant differences between zQ175 and zQ175:CK2α'$^{(+/-)}$ at 3 months (**Fig. 5A**). At 12 months, both genotypes showed a reduced latency to fall on day 1 of training compared to 3-month-old mice (**Fig. 5A, B)**. However, at the end of the test, zQ175:CK2α'$^{(+/-)}$ mice showed a significant improvement compared to zQ175 mice, reaching a similar latency to fall as observed at 3 months of age (**Fig. 5A, B**). For the beam walk test, which evaluates whole body balance, we performed analyses in four different beams with different degrees of challenge (medium square; the less challenging, medium round, small square and small round; the most challenging) and recorded the time to cross and number of foot slips (defined as when the hind paw slipped below the midline of beam) during crossing (**Fig. 5C-F**). At 3 months of age there were no differences between the two genotypes in terms of time it took to cross the beam. The average time for each of the four types of beams was 15 seconds (**Fig. 5C**). At 12 months of age zQ175 mice showed an increase in time to cross the beam, on average 38 sec, indicating a worsening in motor performance (**Fig. 5D**). Conversely, latency to cross the beam was significantly improved in zQ175:CK2α'$^{(+/-)}$ mice across all beams, suggesting an amelioration of the motor impairment found in age-matched HD mice (**Fig. 5D**). Interestingly, when the number of foot slips was assessed, zQ175:CK2α'$^{(+/-)}$ mice showed a significant reduction compared to zQ175 mice at 3 months but only in the most challenging beam (small round) (**Fig. 5E**). At 12 months the number of foot slips increased for both genotypes compared to 3 months, especially in the most challenging beams (small square and small round), but zQ175:CK2α'$^{(+/-)}$ mice showed a significant improvement compared to

HD mice (**Fig. 5F**). However, other motor tests such as open field or cylinder test did not show a significant difference between zQ175 and zQ175:CK2α'$^{(+/-)}$ mice (**Fig. S6A-F**).

In addition to motor deficits, loss of cognitive function is a prominent characteristic of HD. Cognitive functions affected in HD include executive dysfunction, inefficiencies in attention, and working and spatial memory deficits (Paulsen 2011, Glikmann-Johnston et al. 2019, Stout et al. 2012). Cognitive dysfunction is often reported prior to overt motor symptoms in patients with HD (Stout et al. 2012, Harrington et al. 2012, Paulsen 2011), but it usually manifests after motor symptom onset in murine models of HD (Farrar et al. 2014, Heikkinen et al. 2012). Cognitive function in heterozygous zQ175 mice progressively decreases with age, beginning as early as 7 months with robust cognitive impairment at 10-12 months of age (Curtin et al. 2015, Southwell et al. 2016, Piiponniemi et al. 2018). To assess whether cognitive behavior was altered as a function of CK2α' in HD mice, we performed tests to evaluate associative learning (fear conditioning), spatial learning and memory (Barnes maze, BM), cognitive flexibility (BM reversal) and spatial working memory (Y radial arm maze) by comparing zQ175 and zQ175:CK2α'$^{(+/-)}$ mice at 12 months of age. No significant differences were observed in fear conditioning, BM or Y maze between the two genotypes (**Fig. S6G, H, S7**). In the case of BM reversal, no significant differences were observed in either the total distance traveled searching for the target zone or the mean distance from the target (**Fig. S7G, H**). However, when evaluating the latency to reach the entry zone for the first time during BM reversal, we observed a significant increase in zQ175:CK2α'$^{(+/-)}$ mice compared to zQ175 (**Fig. S7I**) suggesting a possible worsening in the cognitive flexibility of learning a new location. This observation suggests that the positive effects

of CK2α' depletion on motor behavior may not translate to cognitive functions. This could be explained by the synergistic contribution of different brain regions to the execution of these cognitive tasks. The cognitive tests performed in this study, although useful to study striatum contribution to specific forms of memory and learning, are predominantly driven by the hippocampus and frontal cortex. CK2α' is predominantly expressed in the cortex and hippocampus under physiological conditions, indicating an important role of this protein in those brain regions (Ceglia, Flajolet, and Rebholz 2011, Rebholz et al. 2013). Since pathological up-regulation of CK2α' in HD seems to be constrained to the striatum (**Fig. 1D**), it is possible that systemic depletion of CK2α' in zQ175 mice could impair physiological functions of this protein in other brain regions where its levels are not altered.

## Gene expression of synaptic genes regulated by alpha-synuclein is rescued by CK2α' depletion in zQ175 mice

To elucidate the mechanism by which CK2α' contributes to HD we investigated which molecular pathways associated with HD could be specifically affected by CK2α' haploinsufficiency by conducting RNAseq analysis in the striatum of WT, zQ175, CK2α'$^{(+/-)}$ and zQ175:CK2α'$^{(+/-)}$ mice at 12-14 months (n=5 mice/genotype for WT, zQ175 and zQ175:CK2α'$^{(+/-)}$ and n=3 mice for CK2α'$^{(+/-)}$, with a female (F)/male (M) ratio: 4F/1M WT, 1F/2M CK2α'$^{(+/-)}$, 2F/3M zQ175, 4F/1M zQ175:CK2α'$^{(+/-)}$). Weighted Gene Co-Expression Network Analysis (WGCNA) revealed that the mice transcriptome could be clustered into 20 gene co-expression modules given the sample phenotypes

(**Fig. S8, Table S1**). Out of the 20 modules, 9 modules (Blue, Black, Green, Greenyellow, Lightyellow, Yellow, Purple, Red and Grey) showed a significant difference of eigengene expression between zQ175 and WT mice in Kruskal-Wallis test (p value < 0.05) (**Fig. S9A, Table S2**). Further evaluation of those 9 modules revealed 2 modules (Greenyellow, 255 genes and Red, 639 genes) are also significantly different between zQ175 and zQ175:CK2α'$^{(+/-)}$ mice (p value < 0.05) (**Fig. 6A, Table S2**). Plots of module eigengene expression confirmed that Greenyellow (**Fig. 6B)** and Red modules (**Fig. S8**) are more consistent in the expression contrast between zQ175 mice and the rest of the genotypes than all other modules. These two modules were then imported into Ingenuity pathway analysis (IPA) to identify key pathways and genes potentially regulated by CK2α' in HD. The five most significant canonical pathways in the Greenyellow module were synaptogenesis signaling pathways (p-value 1.68E-06), Ephrin A signaling (p-value 7.84E-05), glutamate receptor signaling (p-value 1.98E-04), axonal guidance signaling (p-value 7.13E-04) and G-protein coupled receptor (GPCR) signaling (p-value 1.14E-03) (**Fig. 6C**), all of which have been previously implicated in HD pathogenesis (Langfelder et al. 2016, Hodges et al. 2006, Diaz-Castro et al. 2019). In the Red module, the top five most significant pathways were brain expressed X-linked (BEX) signaling pathway (1.05E-05), involved in cancer and apoptosis, phagosome maturation (3.68E-05), synaptogenesis (8.72E-05), GABA receptor signaling (2.81E-04) and insulin secretion (4.09E-04) (**Fig. S9B**). Due to the higher significance of the Greenyellow over the Red module, we decided to focus our analyses on the Greenyellow module. Additional Gene Ontology (GO) annotation of cellular

components indicated that Greenyellow genes are significantly enriched in synaptic components (**Fig. 6D**).

To directly visualize the gene composition of the Greenyellow module, we generated a connectivity diagram depicting genes with the highest connectivity (hubs). For clarity only 15% of the most highly connected members of the module were depicted and the size of the circles was scaled by the absolute value of the mean log2-fold change between zQ175 and zQ175:CK2α'$^{(+/-)}$ mice (**Fig. 6E**). All hub genes except one were up-regulated in zQ175 mice compared to zQ175:CK2α'$^{(+/-)}$. We found that the three most connected genes within the hub were Nfib (CCAAT-Box-Binding Transcription Factor), Slit1 (Slit Guidance Ligand 1), and Ncald (Neurocalcin delta). Nfib is involved in forebrain development and is essential during embryogenesis (Steele-Perkins et al. 2005). Slit1 is involved in cell migration and axonal guidance and its up-regulation was previously associated with "poor" behavior and a worse prognosis in the R6/1 mouse model (Gallardo-Orihuela et al. 2019). Ncald is involved in the regulation of G protein-coupled receptor signal transduction and is also implicated in the regulation of multiple endocytosis-dependent neuronal functions, synaptic vesicle recycling, and neurotransmitter release (Vercauteren et al. 2007, Yamatani et al. 2010, Riessland et al. 2017). Interestingly, Ncald is situated on a locus that has been associated with earlier clinical onset of HD in GWAS studies (Consortium 2015). Although the relationship between these genes and CK2α' is unknown, our data suggests a potential connection between CK2α' and these signaling pathways.

To complement our WGCNA result and better understand which specific genes were more impacted in their expression by CK2α' depletion, we examined the Differential

Gene Expression (DGE) between control mice (WT and CK2α'$^{(+/-)}$) and HD mice (zQ175 and zQ175:CK2α'$^{(+/-)}$) (**Table S3**). As expected, we observed almost no detrimental effects of CK2α' depletion in CK2α'$^{(+/-)}$ mice compared to WT (the number of DGEs is n=11). The DGEs between WT and zQ175 mice confirmed a large transcriptional dysregulation (n=885 genes, Q<0.1) (**Fig. S9C, Table S3**), as previously reported (Langfelder et al. 2016). We also compared our data set with the previously published RNA-seq results for the zQ175 mouse (Langfelder et al. 2016) and observed a large number of overlapping genes (**Fig. S9D**). Interestingly, the DGE between zQ175:CK2α'$^{(+/-)}$ vs WT only reported 123 genes, indicating an amelioration in the global transcriptional dysregulation compared to zQ175 mice (**Fig. S9E, F**).

Since CK2α' depletion significantly reduced the levels of inflammatory cytokines (**Fig. 2**), decreased astrocyte proliferation, and reduced the number of C3d+ astrocytes (**Fig. 3**), we specifically looked for microglial and astrocytic inflammatory RNA signatures (Diaz-Castro et al. 2019, Liddelow et al. 2017) in our data set. However, we failed to find significant changes in the expression of these gene signatures even when comparing WT vs zQ175 mice (**Fig. S10A, B, Table S4, S5**). Similar results were found by Castro-Diaz et al., when conducting RNA-seq analysis in brains from patients with HD and in striatum from R6/2 and zQ175 mice, which demonstrates an absence of transcriptional changes that are characteristic of inflammatory microglia or A1/A2 astrocytes in these different models of HD (Diaz-Castro et al. 2019, Al-Dalahmah et al. 2020). However, we recapitulated some findings observed by Castro-Diaz et al, and found transcriptional changes for some genes of the HD-associated astrocyte molecular signature in the zQ175 mice, indicative of astrocytic dysfunction (Diaz-Castro et al. 2019) (**Fig. S10C**).

Notably, these changes were not observed when comparing zQ175:CK2α'$^{(+/-)}$ vs WT mice.

The DGEs analyzed between zQ175 and zQ175:CK2α'$^{(+/-)}$ mice revealed a specific set of 39 genes with significance (FDR<0.1) (**Fig. 6F, Table S6**), including Csnk2a2 (CK2α' gene) as a positive control. At least 40% of the 39 genes (n=16) were related with synaptic functions (**Fig. 6F, Table S6**). We also found that 10 of the most differentially expressed genes within the 39 gene set were present in the Greenyellow module (**Fig. 6F, Table S1, S6**). Notably, we found that Ncald, one of the most connected genes within the Greenyellow module, was also one of the most dysregulated genes between zQ175 and zQ175:CK2α'$^{(+/-)}$ mice. The expression of Ncald, associated with early HD onset (Consortium 2015), was upregulated in zQ175 mice vs. WT but its expression was decreased to nearly WT levels in the zQ175:CK2α'$^{(+/-)}$ mouse. This change could have a profound impact on a large number of genes, as indicated by WGCNA, and could contribute to the improved phenotype of the zQ175:CK2α'$^{(+/-)}$ mice. We performed IPA on the 39 genes set to query for biological meaning and found that the most significant canonical pathway was for glutamate receptor signaling (p-value 2.09E-03), one of the pathways identified in the Greenyellow module (**Fig. 6A**). These pieces of data confirm the contribution of CK2α' to the regulation of genes related to excitatory synaptic transmission in HD, as it is manifested by the increase in mEPSC frequency observed in zQ175:CK2α'$^{(+/-)}$ mice (**Fig. 4F, G)**.

When looking at the most significant upstream regulators identified by IPA of both the Greenyellow module and the 39 gene set identified by DGE, we found SNCA (alpha-synuclein) (p-value 9.10E-11 and 1.03E-07, respectively). alpha-Synuclein (α-syn) is a

cytoplasmic protein associated with onset and progression of Parkinson's disease, and it has also been associated with HD. A previous report showed α-syn colocalizes with polyQ inclusions in the striatum of R6/1 mice (Tomás-Zapico et al. 2012). α-syn seems to act as an additional mediator of polyQ toxicity since it is induced in plasma from patients with HD and its deletion decreased mHTT aggregation, body weight loss and early motor phenotype of HD mice (Tomás-Zapico et al. 2012, Breza et al. 2020). However, the mechanism of action of α-syn in HD has not yet been determined and therefore, the connection between α-syn, CK2α' and HD transcriptional deficits is new. α-Syn is primarily in the cytosol and interacts with cell membranes, but it has been reported to regulate gene expression (Decressac et al. 2012, Davidi et al. 2020). Specifically, phosphorylated forms of α-syn associated with α-syn aggregation have been seen to localize in the nucleus, where it could interfere with transcription (Fujiwara et al. 2002, Schell et al. 2009, Schaser et al. 2019). Aggregation of α-syn and PD has been linked to the activation of CK2 and CK2-dependent phosphorylation (Takahashi et al. 2007, Lee et al. 2004). IPA connected α-syn with some of the most dysregulated genes in the set of 39 genes including Grm2, Slc17a7, C1ql3 and the transcription factors Tbr1 and Nr4a2 (**Fig. 6G**). Tbr1 is a transcriptional repressor involved in neurodevelopment, neuronal migration, and axonal projection (Huang and Hsueh 2015). Nr4a2 is a nuclear receptor, also known as Nurr1, essential for the development and specification of midbrain dopamine neurons and regulated by α-syn (Decressac et al. 2012). Nr4a2 expression is found to be directly induced by various stimuli such as inflammatory signals and cytokines, and although its up-regulation is often associated with protective effects, it is also an indicator of a neuroinflammatory response (Jeon et

al. 2020). Overall, these data suggest that CK2α' could be modulating synaptic activity and neuroinflammation by controlling the activity of α-syn and their corresponding targets.

**Striatal synucleinopathy is found in zQ175 mice and is reduced by CK2α' depletion**

We explored whether CK2α' is involved in the modulation of α-syn in HD. We performed IF analyses to evaluate HTT inclusions (HTT+) and α-syn (4D6+) distribution within the striatum of WT, zQ175 and zQ175:CK2α' $^{(+/-)}$ mice at 12 months (**Fig. 7A**). We observed that HTT aggregates localized in the nucleus as well as outside the nuclear compartment in both zQ175 and zQ175:CK2α'$^{(+/-)}$ mice (**Fig. 7A**). Cytoplasmic HTT aggregates were reduced in zQ175:CK2α'$^{(+/-)}$ compared to zQ175 mice, consistent with previous studies (Gomez-Pastor et al. 2017), although no significant differences were observed in the number of nuclear HTT aggregates (**Fig. 7B, C**). On the other hand, the total amount of α-syn as well as the subcellular distribution was similar between all genotypes, we did not observe colocalization between HTT aggregates and α-syn, and no clear nuclear α-syn localization was detected (**Fig. 7A, D, E**).

We then evaluated phosphorylated α-syn, since this is a marker of synucleinopathy and accounts for 90% of the α-syn observed in Lewy bodies (LB)(Fujiwara et al. 2002). Phospho-Ser129-α-syn (pS129-α-syn) plays an important role in the regulation of α-syn aggregation, LB formation, and neuronal degeneration (Oueslati 2016). CK2 has been previously associated with α-syn phosphorylation and aggregation. Therefore, we

563 evaluated whether pS129-α-syn was altered in HD and whether CK2α' could influence
564 its accumulation. We first observed that the levels of pS129-α-syn were significantly
565 induced in the striatum of zQ175 mice at 12 months compared to WT, indicating signs
566 of synucleinopathy in HD. Interestingly, the levels of pS129-α-syn were significantly
567 reduced in zQ175:CK2α'$^{(+/-)}$ mice compared to zQ175 while no significant differences
568 were observed with WT mice (**Fig. 7F-I**). We also observed that pS129-α-syn was
569 detected in the nucleus of striatal HD cells while no nuclear localization of pS129-α-syn
570 was found in the zQ175:CK2α'$^{(+/-)}$ mouse (**Fig. 7J-K**). These phosphorylated species
571 were not detected with the pan reactive α-syn 4D6 antibody (**Fig. 7A**), which detects the
572 carboxy-terminus domain of α-syn and is often buried in α-syn fibril aggregates,
573 suggesting that nuclear pS129-α-syn could be aggregated.

574 In addition, we observed that pS129-α-syn colocalized with both cytoplasmic and
575 nuclear HTT aggregates in zQ175 mice while only cytoplasmic colocalization was
576 observed in zQ175:CK2α'$^{(+/-)}$ mice (**Fig. 7J-K**). The differential accumulation of nuclear
577 pS129-α-syn between zQ175 and zQ175:CK2α'$^{(+/-)}$ mice could be responsible for the
578 transcriptional changes observed between these two genotypes (**Fig. 6**) as well as for
579 the neuropathological and behavioral improvement observed in zQ175:CK2α'$^{(+/-)}$ mice
580 (**Figs. 2-5**). Overall, these data demonstrated that pathological upregulation of CK2α' in
581 HD is associated with increased pS129-α-syn and therefore suggested that HD
582 symptomatology could be a combination of mutant HTT aggregation as well as α -
583 synucleinopathy.

584

## Discussion

Increased protein kinase CK2 activity has been associated with detrimental effects in protein homeostasis and neuroinflammation in different neurodegenerative diseases including AD, PD, and ALS (Castello et al. 2017). However, the role of CK2 in HD remained unclear. This study demonstrated the adverse effects of the catalytic subunit CK2α', on neuroinflammation, protein aggregation, neuronal function and motor behavior in the zQ175 HD mouse model and consolidated the important contribution of CK2α' to HD pathogenesis. We also found that this contribution is mediated, at least in part, by the ability of CK2α' to phosphorylate α-syn and induce striatal synucleinopathy (**Fig. 7L**).

We previously showed that CK2α' levels were induced in the striatum of patients with HD, in MSN-like human iPSCs derived from patients with HD, and in zQ175 mouse MSNs (Gomez-Pastor et al. 2017). CK2α' upregulation was associated with HD pathogenesis since CK2α' genetic knockdown in different HD cell models resulted in decreased HTT aggregation and increased cell viability (Gomez-Pastor et al. 2017). However, other studies using CK2 inhibitors suggested CK2 induction as a protective mechanism in HD (Atwal et al. 2011, Fan et al. 2008b). Atwal et al., indicated that CK2 participates in HTT phosphorylation and nuclear localization while its pharmacological inhibition decreased HTT phosphorylation and increased cell death (Atwal et al. 2011). Other studies using ectopic overexpression of mHTT fragments combined with different CK2 inhibitors resulted in NMDA mediated toxicity (Fan et al. 2008a). However, several experimental limitations are associated with these conflicting studies. These include the exclusive use of cell models, use of CK2 inhibitors with poor selectivity and high toxicity

(Mikula et al. 2010), and absence of genetic evidence to demonstrate the specificity of the inhibitors used as well as the differential contribution between CK2α or CK2α' subunits. We have now confirmed that CK2α' upregulation in HD is detrimental and contributes to HD onset and progression.

Our study demonstrated that reducing levels of CK2α' by removing one allele of the Csnk2a2 (CK2α') gene in the zQ175 heterozygous HD mouse model (zQ175:CK2α'$^{(+/-)}$) had significant and long-term benefits in several HD-related phenotypes. Our work showed that CK2α' depletion significantly altered the production of several pro-inflammatory cytokines (i.e. IL-1α, IL-1β, TNF-α, INF-g and IL-6) in the striatum of symptomatic zQ175 mice. HTT aggregates as well as components of dead neurons trigger the activation of pro-inflammatory cytokines that amplify inflammatory signals and result in increased neurotoxicity (Crotti and Glass 2015). Similarly, α-syn has been shown to influence cytokine production. Studies in THP-1 cells overexpressing α-syn and rats injected with an adeno-associated virus expressing α-syn (AAV-SYN) showed the activation of cytokine expression, particularly TNF-α, IL-1β and IFN-γ (Chung et al. 2009). α-syn-mediated inflammation is dependent on MAPKs and NF-kβ activation (Hoenen et al. 2016). The benefits of reducing neuroinflammation in HD have been shown in R6/2 mice intracranially injected with a TNF-α inhibitor, which resulted in a significant increase in neuronal density and improved motor function (Hsiao et al. 2014). We obtained similar results when reducing the expression of CK2α', suggesting CK2α' as a potential upstream regulator of neuroinflammation in HD. It is possible that CK2α' regulates neuroinflammation in HD directly by phosphorylating and controlling NF-kβ function, as previously shown in cancer cells (Kato et al. 2003), or indirectly by

631 decreasing HTT aggregation and/or increasing α-syn phosphorylation. In addition, CK2
632 activity is also regulated by IL-1β, TNF-α, and IFN-γ (Singh and Ramji 2008),
633 establishing a positive regulatory feedback loop that helps perpetuate chronic
634 neuroinflammation in the HD brain.

635 Neuroinflammation is a coordinated response to brain toxicity involving the activation of
636 microglia and astrocytes. Increased reactive microglia were reported in numerous HD
637 mouse models (Pavese et al. 2006, Savage et al. 2020, Franciosi et al. 2012), in pre-
638 symptomatic patients with HD (Pavese et al. 2006, Tai et al. 2007), and are often
639 associated with increased pro-inflammatory cytokines (Crotti and Glass 2015). Although
640 there is mounting evidence that microglia play an important role in HD pathogenesis,
641 the extent of their contribution and the exact timing at which activated microglia are
642 essential in HD is still unclear. We observed inconsistent results when analyzing the
643 levels of Iba1 (marker of reactive microglia) in symptomatic zQ175 mice. While IB
644 showed increased levels of Iba1 in HD groups (CK2α'$^{(+/+)}$ and CK2α'$^{(+/-)}$) indicating
645 microgliosis, IF analysis did not show significant changes in either the number nor the
646 area of reactive microglia between WT and HD groups, despite cytokine expression
647 being significantly different among them. Our data is consistent with a recent report
648 suggesting the absence of significant microgliosis in symptomatic zQ175 mice (Diaz-
649 Castro et al. 2019). Similar results were obtained in the R6/2 mice using a combination
650 of light and transmission electron microscopy, where increased reactive microglia and
651 microglia phagocytic activity were preferentially induced at pre-symptomatic stages
652 (Savage et al. 2020). Therefore, although microglia may play an important role during
653 early HD pathogenesis, their role could become less relevant at later stages of the

654 disease (Petkau et al. 2019). This data suggest that increase inflammatory cytokines
655 observed in symptomatic zQ175 mice could be produced by cells other than microglia.

656 On the other hand, increased number of astrocytes and astrocytic pathology, which are
657 features of astrogliosis (Anderson, Ao, and Sofroniew 2014, Sofroniew 2009), are more
658 consistent with HD progression. While microglia activation may influence HD motor
659 onset, astrocyte pathology is more likely to contribute to the continued progression and
660 worsening of the HD phenotype (Wood et al. 2019). We found decreased number of
661 astrocytes in zQ175:CK2α'$^{(+/-)}$ mice compared to zQ175 mice at all tested ages.
662 Decreased number of astrocytes in the striatum also correlated with decreased mIns
663 levels assessed by $^{1}$H-MRS *in vivo*. Although it is unknown how CK2α' influences
664 astrocyte proliferation, it has been shown that specific cytokines like TNF-α and IL-6
665 have a proliferative effect on astrocytes (Selmaj et al. 1990) and therefore CK2α'-
666 mediated changes in these cytokines could be responsible for these phenotype in HD
667 mice. Decreased astrocytes in zQ175:CK2α'$^{(+/-)}$ mice were also accompanied by a
668 decrease in the total levels of C3d and in the proportion of C3d immunoreactive
669 astrocytes compared to zQ175 mice. Accumulation of C3 and C3d in HD astrocytes is
670 canonically considered a marker of astrocytic pathology associated with
671 neuroinflammation although it can also be detected in neurons and myelin in HD human
672 striatum (Liddelow et al. 2017, Singhrao et al. 1999, Diaz-Castro et al. 2019). In AD,
673 expression of C3d in astrocytes is induced by neuroinflammatory processes triggered
674 by amyloid-beta and its activation contributes to protein aggregation and cell death (Lian
675 et al. 2016). Liddelow et al., recently reported that astrocytes react to the presence of
676 specific cytokines, such as IL-1α, TNF-α and C1q, by changing their transcriptional

677 program and adopting a neurotoxic phenotype (type A1) which is also characterized by
678 the accumulation of C3d (Liddelow et al. 2017). Previous transcriptomic studies in
679 purified HD astrocytes (Diaz-Castro et al. 2019) and our own RNA-seq data have failed
680 to identify the presence of transcriptional changes characteristic of A1 astrocytes but
681 instead revealed a transcriptional signature related to astrocytic dysfunction that is yet
682 associated with the activation of C3d. It is still unknown how CK2α'-mediated decrease
683 in IL-1α and TNF-α and other cytokines could influence C3d expression in astrocytes
684 and astrocytic pathology.

685 Pro-inflammatory cytokines and astrocyte dysfunction negatively impact neuronal
686 activity and synaptic plasticity. Increased IL-1β , TNF-α and IL-6 can alter inhibitory
687 synaptic strength as well as glutamatergic transmission (Vezzani et al. 2008) and are
688 also associated with structural and functional disruption of synaptic compartments
689 (Mottahedin et al. 2017). Similarly, astrocyte dysfunction in HD contributes to reduced
690 striatal glutamatergic transmission and spine density, ultimately decreasing MSN
691 excitability (Wood et al. 2019, Khakh et al. 2017). We showed that CK2α'-dependent
692 decrease of pro-inflammatory cytokines and astrogliosis in the HD striatum correlated
693 with increased expression of synaptic proteins (i.e. PSD-95 and Darpp-32) and
694 improved AMPA-mediated synaptic transmission. This is consistent with previous
695 findings that showed rescue in the expression of synaptic proteins and synaptic activity
696 in the striatum when conditionally deleting mHTT from astrocytes and improving
697 astrocytes health in the BACHD mice (Wood et al. 2019). However, whether decreased
698 astrocytic pathology contributes to improved neuronal activity in zQ175:CK2α'$^{(+/-)}$ mice is
699 yet to be determined.

In contrast to CK2α, which is an essential protein with hundreds of targets (Bian et al. 2013, Franchin et al. 2018, Olsen et al. 2010), CK2α' has very few substrates identified (Bian et al. 2013). We previously showed the stress protective transcription factor HSF1 is a substrate of CK2α' (Gomez-Pastor et al. 2017). HSF1 is the master regulator of protein homeostasis in mammalian cells and has also been linked to the regulation of anti-inflammatory and synaptic genes (Gomez-Pastor, Burchfiel, and Thiele 2017). We recently demonstrated that CK2α' phosphorylates HSF1, signaling HSF1 for proteasomal degradation and influencing chaperone expression and HTT aggregation in cells and in HD mice (Gomez-Pastor et al. 2017). Our RNA-seq analysis validated the increased expression of chaperones like Hsp70 and Hsp25 in the zQ175:CK2α'$^{(+/-)}$ mice, consistent with previous findings (Gomez-Pastor et al. 2017). However, WGCNA and DGE did not reveal global changes in specific transcriptional pathways associated with HSF1 between zQ175 and zQ175:CK2α'$^{(+/-)}$ at a symptomatic age. Instead WGCNA showed two different modules (Greenyellow and Red) primarily corresponding to signaling pathways related to synaptogenesis and glutamate receptor signaling. SNCA (α-syn) was indicated by IPA as one of the top putative upstream regulators of the CK2α'-mediated transcriptional changes observed by WGCNA and DGE analyses. Our data strongly suggested a potential role of CK2α' in regulating α-syn function. Although α-syn is not a transcription factor, several reports have shown the ability of α-syn to modulate the expression of other transcription factors such as Nurr1, which is involved in the regulation of inflammation and is differentially expressed between zQ175 and zQ175:CK2α'$^{(+/-)}$ mice (Davidi et al. 2020, Decressac et al. 2012). α-syn also regulates the activation of NF-kβ by regulating MAPKs (Hoenen et al. 2016). α-syn aggregation is

723 thought to be a key process in PD and other synucleinopathies and is promoted by the
724 presence of high levels of α-syn phosphorylation and ubiquitylation (Fujiwara et al.
725 2002, Anderson et al. 2006). pS129-α-syn phosphorylation regulates neurotransmitter
726 uptake, notably dopamine, as well as glutamate release, thereby playing an important
727 role at synaptic terminals and modulating synaptic plasticity (Hara et al. 2013, Fujiwara
728 et al. 2002).

729 The specific contribution of α-syn dysregulation in HD has yet to be determined. It is
730 known that α-syn participates in HD pathogenesis since α-syn KO mice have decreased
731 mHTT aggregation and attenuated body weight loss and motor symptoms of R6/1 mice
732 (Tomás-Zapico et al. 2012). Interestingly, aggregation of α-syn and consequent
733 synucleinopathy in PD has been linked to the activation of CK2 and CK2-dependent
734 phosphorylation (Takahashi et al. 2007, Lee et al. 2004). Here we showed increased
735 pS129-α-syn in the striatum of symptomatic HD mice and increased localization of this
736 phosphorylated form in the nucleus. Furthermore, we demonstrated that CK2α' is most
737 likely to be involved in this process. Decreased phosphorylation and accumulation of
738 pS129-α-syn in the nucleus could be responsible for the rescue of α-syn-associated
739 transcriptional alterations and the improvement on synaptic function, cytokine
740 expression and astrocytic pathology seen in zQ175:CK2α'$^{(+/-)}$ mice. Overall, these
741 results provided strong evidence for CK2α' playing an important role in many aspects of
742 HD pathogenesis, supporting its potential as a therapeutic target in HD. However,
743 further experiments will be necessary to decipher the mechanism by which CK2α'-
744 mediated α-synucleinopathy contributes to HD and to tease apart the differential

745 contribution of HTT aggregation and α-syn pathology to the symptomatology, onset and
746 progression of HD.

747

748 **Figure Legend**

749

750 **Figure 1**. **CK2α' levels progressively increase in the striatum of zQ175 and**
751 **correlate with HTT aggregation and neuronal loss.** ***A***, ***B****,* HTT aggregates detected
752 with EM48, anti-HTT antibody, increases in an age-dependent manner in zQ175 HD
753 compared with WT (*n*=6). ***C***, ***D***, Antibodies against neuronal marker NeuN reveals a
754 significant loss of neurons at late stage in zQ175 (*n*=6). ***E***, ***F***, Quantification of CK2α'
755 levels by immunofluorescence analysis (n=6) show CK2α' is highly expressed with age
756 in zQ175. ***G****,* CK2 α' mRNA levels analyzed by RT-qPCR measurements at 6 months
757 old mice, with restricted expression in the striatum. Data are normalized with GAPDH
758 and WT (n = 3 biological replicates with three technical replicates per experiment). ***H***, ***I***,
759 Linear regression analysis reveals a significant increase in slope between CK2α' levels
760 and HTT aggregation (***H***), and decrease in slope between CK2α' levels and NeuN
761 immunoreactivity (***I***) in HD. The Pearson correlation coefficient (ρ) and $R^2$ are indicated.
762 Data are mean ± SD with significance determined by one-way ANOVA Dunnett's post-
763 hoc test in ***B*** and ***F*** and two-way ANOVA Tukey post-hoc test in ***D*** and ***G***. n.s = not
764 significant. Scale bar, 50 μm. See also Figure S1.

765

**Figure 2**. **Expression of pro-inflammatory cytokines in the striatum of zQ175 is decreased by reduction in CK2α'**. ***A***, RT-qPCR analysis for CK2α' and IL-6 in immortalized embryonic striatal cells ST*Hdh*$^{Q7/Q7}$ (control) and ST*Hdh*$^{Q111/Q111}$ (HD). Data were normalized with GAPDH and using control cells as a reference (n=4 independent experiments) ***B***, siRNA knockdown of CK2α' for 24 h in ST*Hdh*$^{Q111/Q111}$ cells induces IL-6 downregulation. Data were normalized with GAPDH and relativized to non-targeting control siRNA-treated cells (scramble), (*n* = 3 independent experiments). (***A***, ***B***) Data are mean ± SEM with significance determined by unpaired Student's t-test. ***C***, ***D***, Representative immunofluorescence images (***C***) and quantitative analysis (***D***) demonstrate high expression of CK2α' in striatal MSNs immunostained for Ctip2, a specific MSN marker, in zQ175 HD at 12 months of age. Genetic deletion of CK2α' $^{(+/-)}$ lowered the expression of CK2α' (*n* = 3 mice/genotype). Scale bar, 50 µm. ***E***, ***F***, Representative immunoblotting of mouse cytokine array panels in WT, HD, and zQ175:CK2α'$^{(+/-)}$ at 12-14 months of age showed increased levels of pro-inflammatory cytokines from striatum in HD compared with WT. In contrast, CK2α' haploinsufficiency reduced the levels of cytokines compared with HD (*n* = 6 WT; 6 HD; 6 zQ175:CK2α'$^{(+/-)}$). ***G-I***, Iba1 quantification in the striatum of 12 months old WT, zQ175 and zQ175:CK2α' from images in ***G*** using the Image J software. Density (***H***) and the average area (***I***) of Iba1+ microglia between groups are unchanged across genotypes (*n* = 4 mice/genotype). Scale bar, 100 µm. Error bars denote ± SD, values were analyzed by Student's t test in ***A***, ***B*** and ***F***, and one-way ANOVA and Tukey post-hoc test in ***D***, ***H*** and ***I***. **p* represent p-values comparing zQ175 and WT, #*p* are p-values comparing zQ175 and zQ175:CK2α'$^{(+/-)}$. See also Figures S2 and S3.

**Figure 3**. **Decreased CK2α' ameliorated astrocyte pathology in zQ175 mice**. ***A***, Representative images of striatum sections from 12-months-old mice immunostained for CK2α' and glutamine synthetase (GS, an astrocytic marker). Both CK2α' and GS are strongly upregulated in zQ175 compared with WT, but downregulated in zQ175:CK2α'$^{(+/-)}$ compared with zQ175. ***B***, Quantification of GS+ cells from images in ***A*** indicated an increase in astrocytes number in zQ175 and reduction in zQ175:CK2α'$^{(+/-)}$ compared with WT and zQ175, at all ages (*n* = 5 mice per genotype were analyzed at all ages). ***C***, Representative coronal images of brain scans in 9.4T magnet showing the striatum voxel (green box) for MRS acquisition from each genotype at 22 months of age. ***D***, *myo*-inositol (Ins) quantification shows elevated concentrations in zQ175 compared with WT, whereas low Ins is seen in zQ175:CK2α'$^{(+/-)}$ compared with zQ175 (*n* = 4 WT; 4 zQ175; 6 zQ175:CK2α'$^{(+/-)}$). ***E*** – ***G***, representative immunofluorescence analysis of C3d costained with GS in the striatum of 12 months old mice (***E***) demonstrate higher abundance of C3d (***F***) and C3d+ GS+ double-positive cells (***E***; white arrow, ***G***) in zQ175 compared with WT, whereas lower abundance in zQ175:CK2α'$^{(+/-)}$ compared with zQ175 (*n* = 5 mice/genotype). ***E'***, Higher magnification of the outlined section in ***E*** shows a representative view of a single astrocyte immunolabeled with C3d and GS. DAPI is used for nuclear staining. Scale bars, 50 μm. Error bars denote ± SD. *p*-values for differences between groups are indicated in each graph and calculated using two-way ANOVA and Tukey post-hoc tests. n.s. = not significant. See also Figure S4.

**Figure 4**. **CK2α' haploinsufficiency increased the frequency of AMPA-mediated miniature excitatory postsynaptic currents (mEPSC) in the dorsolateral striatum of zQ175 mice**. ***A***, Image shows whole-cell patch-clamp recording diagram in acute dorsolateral striatum slices, where Ctip2 labeled MSNs from 12-month-old mice. Scale bar 500 μm, Ctr: Cortex; Str: Striatum. ***B*** – ***D***, Input–output curve (***B***), short-term potentiation measured via paired-pulse facilitation (***C***), and short-term depression analyzed through synaptic fatigue (***D***) reveal that there is no significant difference in evoked synaptic parameters between groups. ***E***, Summarized graph of spontaneous recordings of mEPSCs shows similar amplitude between groups. ***F***, ***G***, Summarized graph (***F***) and representative mEPSC traces (***G***) show a reduction of mEPSC frequency in MSNs from zQ175, but an increase from zQ175:CK2α'$^{(+/-)}$ mice. Error bars denote ± SEM of the number of cells in parentheses from at least 3 different mice by one-way ANOVA with Dunn´s post-hoc. See also Figure S5.

**Figure 5**. **Genetic deletion of CK2α' improved motor deficits in zQ175.** ***A***, ***B***, Rotarod test at 3 and 12 months of age. Latency to fall at 3 months of age was not different between the two groups (***A***), whereas zQ175:CK2α'$^{(+/-)}$ reduced the decline in rotarod performance at 12 months of age compared with HD (***B***). ***C*** – ***F***, Beam walking test at 3 and 12 months of age. The time to cross all beams was not different between the two groups at 3 months of age (***C***), but was shorter in zQ175:CK2α'$^{(+/-)}$ than zQ175 at 12 months of age (***D***). Three-month-old zQ175:CK2α'$^{(+/-)}$ exhibited small number of foot slips while crossing the small round beam compared with HD (***E***), whereas, at 12 months of age, zQ175:CK2α'$^{(+/-)}$ reduced the number of foot slips in both small square

and round beams (***F***). Error bars denote ± SEM and were analyzed by two-way ANOVA with *Sidak's* post-hoc test (n =16-18 per genotype in 3 months analyses and n=6 per genotype in 12 months analyses). n.s = not significant. See also Figures S6 and S7.

**Figure 6**. **Depletion of CK2α' restored the expression of synaptic genes associated with α-syn-dependent regulation in the striatum of symptomatic zQ175 mice**. (***A***) Kruskal-Wallis test of module expressions between zQ175 (HD) mice and zQ175:CK2α'$^{(+/-)}$ mice. The y axis is the negative log transformed p values. (***B***) Expressions of module "Greenyellow" in each mouse sample. (***C***) IPA canonical pathway analysis of module genes for module "Greenyellow". (***D***) Enrichment analysis of GO terms in CC (cellular component) for module genes of module "Greenyellow". (***E***) Network visualization of top 10% connected genes in "Greenyellow" Module. (***F***) Marker genes and their mean log2 fold change between zQ175 and zQ175:CK2α'$^{(+/-)}$ mice compared to WT. (***G***) IPA network analysis of DGEs in zQ175:CK2α' mice showing α-syn as the most significant upstream regulator. See also Figures S8-S10.

**Figure 7. CK2α' modulates α-syn phosphorylation and aggregation in the striatum of zQ175 mice**. ***A-E***, α-syn and HTT aggregates in the striatum of WT, zQ175 and zQ175:CK2α' mice at 12 months old. (***A***) Representative fluorescence immunolabeling of dorsal striatum sections from WT, zQ175 and zQ175:CK2α'$^{(+/-)}$ (n=3 mice per group) showed no colocalization between α-syn and HTT. α-syn showed a cytoplasmic distribution while HTT aggregates were found in both cytoplasm and nucleus. Scale bar,

20 µm. (*a-c*) magnification of images in ***A***. ***B-C*** Number of HTT aggregates, total (***B***) and nuclear (***C***) HTT aggregates calculated using Image J Puncta analysis plugin. A total of three images per brain section and three brain sections per genotype were analyzed (n=27 images, n=3 mice/genotype) showing a reduction in HTT aggregates in zQ175:CK2α'$^{(+/-)}$ mice. ***D***, α-syn immunoblotting from striatum samples at 12 months of age (n=3 mice/genotype), GAPDH is used as loading control. ***E***, α-syn intensity was calculated from images in ***D*** using ImageJ. Data was normalized using GAPDH intensity and relativized to WT levels. Similar α-syn levels were seen across all genotypes. ***F-G***, Fluorescence immunolabeling of pS129-α-syn in the dorsal striatum of WT, zQ175 and zQ175:CK2α'$^{(+/-)}$ (n=3 mice per group), Scale bar, 20 µm, showed increased pS129-α-syn intensity in zQ175 mice compared to WT and zQ175:CK2α'$^{(+/-)}$ mice. (***G***) pS129-α-syn was calculated using Image J from images in F (n=3 mice/genotype, n=27 images per mouse). ***H-I***, pS129-α-syn and CK2α' immunoblotting of striatum samples from 12 months old zQ175 and zQ175:CK2α'$^{(+/-)}$ mice (n=3 mice/group). (***I***) Levels of pS129-α-syn and CK2α' were calculated using Image J from immunoblotting images in ***H*** and showed a parallel decrease of pS129-α-syn and CK2α' levels in zQ175:CK2α'$^{(+/-)}$ compared to zQ175 mice. ***J-K***, Representative fluorescence immunolabeling of dorsal striatum sections from zQ175 and zQ175:CK2α'$^{(+/-)}$ (n=3 mice/group) showed pS129-α-syn colocalizes with HTT aggregates and accumulates in the nucleus. All data are mean ± SEM. Statistical analyses were conducted by one-way ANOVA in ***B***, ***C***, ***E***, ***G*** and ***K*** and Student's t-test in ***I. L***, Working model for the role of CK2α' in HD.

## Supplementary Material

**Figure S1**. **Loss of MSNs in zQ175 mice are age dependent**. ***A***, Neuronal loss identified by NeuN immunoreactivity is prominent in HD at old age (*n* = 4 WT; 4 zQ175 mice/age). ***B***, ***C***, Representative image (***B***) and quantitative analysis of cells (***C***) from striatum with antibody specific for MSNs, Ctip2, reveal the significant loss of striatal MSNs at 12 months of age (*n* = 4 WT; 5 zQ175). Scale bar, 50 µm. DAPI is used for nuclear staining. Error bars denote ± SD by Student's t-test.

**Figure S2**. **Alteration in CK2α' expression changes cytokine profiles**. ***A***-***C***, Cytokine and chemokine levels in protein extracts from the mouse striatum were assessed by Mouse Cytokine Array Panel A kit (R&D Systems) which detects the relative expression levels of 40 different cytokines (***A***, ***C***). A panel coordinates (***A***) and an example of blotting of cytokine array panels (***B***) show each cytokine has a pair of duplicate spots. ***D***, Bar graph displays mean fold change of cytokine expression in comparison with WT. Although levels of several cytokines are significantly altered in zQ175 and zQ175:CK2α' $^{(+/-)}$, no changes of chemokines are observed (*n* = 3, independent experiments). Error bars denote ± SD by Student's t test.

**Figure S3**. **Decreasing CK2α' in symptomatic zQ175 mice does not reduce microglia activation.** ***A***, ***B***, Western blot analysis of Iba1 in the striatum of 12 months old WT, zQ175 and zQ175:CK2α' mice showed comparable levels between zQ175 and zQ175:CK2α'$^{(+/-)}$ (*n* = 4 WT, 3 zQ175 and 4 zQ175:CK2α'$^{(+/-)}$). GAPDH is used as loading control. (***B***) Iba1 quantification from images in ***A*** using the Image J software. ***C***,

902 ***D***, ***E***, Density (***D***) and the average area (***E***) of Iba1+ microglia between groups are
903 unchanged but a trend toward increased microgliosis in HD (*n* = 4 mice/genotype).
904 Scale bar, 100 µm. Error bars represent mean ± SD, p-values correspond to one-way
905 ANOVA tests.

906

907 **Figure S4**. **CK2α' mice display normalization of striatal myo-inositol, but not**
908 **striatal volume**. ***A***, Localized proton magnetic resonance spectra [LASER sequence,
909 TE= 15 ms, TR= 5 s, 256 transients, 9.4T] obtained at 22 months of age from the
910 striatum of WT, zQ175, and zQ175:CK2α'$^{(+/-)}$ mice (*n* = 4 WT; 4 HD; 6 HD: CK2α' $^{(+/-)}$).
911 Differences in *myo*-inositol (Ins) between WT and zQ175 mice and between zQ175 and
912 zQ175:CK2α'$^{(+/-)}$ mice are shown with arrows. ***B***, Mean concentrations of reliably
913 quantified metabolites in the striatum of WT (black), zQ175 (red), and zQ175:CK2α'$^{(+/-)}$
914 (gray) mice with associated *p* values. ***C***, Dotted line on magnetic resonance images
915 displays the manually traced striatum region of representative mice of each genotype at
916 22 months of age. ***D***, Volumetric analysis of each group showed no significant regional
917 brain atrophy in striatum in HD (*n* = 4 WT; 4 HD; 6 HD: CK2α' $^{(+/-)}$). Error bars denote ±
918 SD by Student's t test (two-tailed, unpaired) (***B***) and one-way ANOVA. *$p$< 0.05. Asc:
919 Ascorbate/vitamin C; tCr: total creatine + phosphocreatine; GABA: gamma-aminobutyric
920 acid; Glc: glucose; Gln: glutamine; Glu: glutamate; tCho: total phosphocholine +
921 glycerophosphocholine; GSH: glutathione; Ins: *myo*-inositol; Lac: lactate; NAA: *N*-
922 acetylaspartate; NAAG: *N*-acetylaspartylglutamate; PE: phosphoethanolamine; Tau:
923 taurine.

924

925 **Figure S5**. **Deficiency in CK2α' expression does not affect MSNs but does**
926 **influence synaptic proteins**. ***A***, ***B***, Representative image (***A***) and quantitative analysis
927 (***B***) from striatum with antibody specific for MSNs, Ctip2, demonstrate the reduced
928 levels of CK2α' by CK2α' haploinsufficiency does not alter MSN number (*n* = 3 HD; 3
929 ZQ175:CK2α'$^{(+/-)}$). Scale bar, 50 µm. ***C***, mRNA levels assessed by RT-qPCR
930 demonstrate that CK2α' haploinsufficiency also does not reverse the reduced
931 expression of Drd1 and Drd2, striatal MSN markers, resulted from high levels of CK2α'
932 in zQ175 HD, but does increase the expression levels of Darpp32 and PSD95, synaptic
933 scaffold proteins (*n* = 4 mice). Error bars denote ± SD by Student's t-test. *p*-values for
934 differences between groups are indicated in each graph. n.s = not significant.

935

936 **Figure S6**. **Genetic deletion of CK2α' does not ameliorate anxiety-like behaviors,**
937 **and spatial working memory of zQ175 HD at 12 months of age**. ***A*** – ***E***, Gross motor
938 performance, exploratory behavior, and anxiety-like behavior were assessed during 30
939 mins in open field test. No differences are identified in distance traveled (***A***) and
940 average locomotion velocity (***C***) between zQ175 HD and ZQ175:CK2α' $^{(+/-)}$. No increase
941 in time spent at the center of the field (***B***) and no decrease in the outer zone of the
942 maze (***D***) suggest no improvement in anxiety-related behavior caused by HD.
943 Representative tracing images (***E***) show the total distance traveled by the subject. Both
944 mice tracks are closely in proximity to the walls of the arena, indicative of increased
945 anxiety-related behavior. ***F*** – ***H***, Parameters of the spontaneous motor activity (number

946 of rears) evaluated by a cylinder test (***F***), and the spatial recognition (number of total
947 arm entries) (***G***) and working memory (spontaneous alternation) (***H***) measured by Y
948 maze in HD: CK2α' $^{(+/-)}$ are not altered compared with HD. (*n* = 6 HD; 6 ZQ175:CK2α' $^{(+/-}$
949 $^{)}$). Error bars denote ± SEM and were analyzed by two-way ANOVA with Sidak's post-
950 hoc test. n.s = not significant.

951

952 **Figure S7**. **CK2α' does not alter cognitive deficits in symptomatic HD mice.** ***A***, ***B***,
953 zQ175 and zQ175:CK2α'$^{(+/-)}$ at 12 months of age display similar freezing time in the
954 cued (***A***) and contextual fear conditioning test (***B***), indicating impairment of fear learning
955 and memory are not altered by CK2α' levels. ***C*** – ***E***, No differences are observed in
956 performance on the Barnes maze (BM) task measured by latency to reach the escape
957 hole (***C***), the mean distance from the target location (***D***), and total distance until escape
958 in training sessions (***E***). ***F*** – ***I***, Results of BM reversal test are similar with those in BM
959 test (***F***, ***G***, ***H***). However, zQ175:CK2α'$^{(+/-)}$ increased escape latency compared with
960 Q175 (***I***). Error bars represent mean ± SEM. Statistical analyses were conducted by
961 ANOVA and *Sidak's* post-hoc test (*n* = 6 mice/genotype). n.s = not significant.

962

963 **Figure S8**. **Expressions of all identified co-expression gene modules from**
964 **WGCNA studies for each mouse sample**. A total of 20 different modules were
965 identified when comparing all the genotypes.

966

967 **Figure S9**. RNA-Seq comparison between samples and with Langfelder et al., 2016.
968 (***A***) Kruskal-Wallis test of module expressions between zQ175 mice and WT mice. (***B***)
969 IPA canonical pathway analysis of module genes for module "Red". (***C***) MA-plot of
970 differential gene expression between HD (zQ175) and WT mice. (***D***) Venn Diagram of
971 differentially expressed genes between HD (zQ175) and WT mice in comparison to
972 Langfelder 2016 data. (***E***) MA-plot of differential gene expression between
973 zQ175:CK2α'$^{(+/-)}$ and WT mice. (***F***) Venn Diagram of differentially expressed genes
974 between zQ175, WT, zQ175:CK2α' and CK2α' mice.

975

976 **Figure S10**. **Marker genes and their expression in RNA-Seq experiments**. (***A***)
977 Microglia known marker genes; A1 inducing microglia markers and reactive microglia
978 markers from Liddelow et al, 2017 in WT, zQ175 and zQ175:CK2α' mice. (***B***) Astrocytes
979 marker genes representative of A1, A2 and pan reactive from Liddelow et al., 2017 in
980 WT, HD and ZQ175:CK2α' mice. (***C***) Marker genes representative of the astrocyte
981 molecular signature in HD (from Diaz-Castro et al., 2019) and their mean log2 fold
982 change in CK2α'$^{(+/-)}$, WT, HD and ZQ175:CK2α' mice zQ175, and ZQ175:CK2α'$^{(+/-)}$
983 mice, normalized to WT mice.

984

985 **Table S1.** WGCNA Modules genes assignment.

986 **Table S2.** WGCNA module names and number of genes per module.

**Table S3.** Differential Gene Expression analyses across the four different genotypes WT, zQ175, CK2α'$^{(+/-)}$ and zQ175;CK2α'$^{(+/-)}$.

**Table S4.** Expression analyses for astrocyte markers of A1, A2 and pan reactive (from Liddelow et al., 2017) in WT, zQ175, CK2α'$^{(+/-)}$ and zQ175;CK2α'$^{(+/-)}$.

**Table S5.** Expression analyses for microglia markers of A1 inducing and reactive microglia (from Liddelow et al., 2017) in WT, zQ175, CK2α'$^{(+/-)}$ and zQ175;CK2α'$^{(+/-)}$.

**Table S6.** Marker genes and their mean log2 fold change between zQ175 and zQ175:CK2α'$^{(+/-)}$ mice compared to WT.

## STAR Methods

## RESOURCE AVAILABILITY

### *Lead Contact*

Further information and requests for resources and reagents should be directed to and will be fulfilled by the Lead Contact, Rocio Gomez-Pastor (rgomezpa@umn.edu).

### *Materials Availability*

This study did not generate new unique reagents.

### *Data and Code Availability*

RNA-seq data set generated in this manuscript has been deposited at GEO on October 28 and it is awaiting confirmation number.

## EXPERIMENTAL MODEL AND SUBJECT DETAILS

### Cell lines

Mammalian cell lines used in this study were the mouse-derived striatal cells STHdh$^{Q7}$ and STHdh$^{Q111}$ (Coriell Cell Repositories). Cell lines were authenticated by immunoblotting for the detection of mutant HTT protein. Cells were grown at 33ºC in Dulbecco's modified Eagle's medium (DMEM, Genesee) supplemented with 10% fetal bovine serum (FBS), 100 U ml$^{-1}$ penicillin/streptomycin and 100 ug ml$^{-1}$ G418 (Gibco), as previously described (Gomez-Pastor et al. 2017).

### Mouse strains

All reported data abides to the ARRIVE guidelines for reporting animal research. For this study we used a full-length knock-in mouse model of HD known as zQ175 on the C57BL/6J background (B6J.zQ175 KI mice (Stock No. 027410)), which harbors a chimeric human/mouse exon 1 carrying an expansion of ~175 CAG repeats and the human poly-proline region (Menalled et al. 2012a). These mice were originally obtained from Dr. Cagla Eroglu (Duke University). WT (C57BL/6) animals were used as controls.

CK2α′ heterozygous mice (CK2α′$^{(+/-)}$) on the 129/SvEv-C57BL/6J background (Taconic Biosciences TF3062) were originally obtained from Dr. Seldin (Boston University) (Xu et al. 1999). CK2α′$^{(+/-)}$ were crossbreed with WT and zQ175 for more than 10 generations prior to select the founder animals of the study. All used mice are in the C57BL/6J background. All mice were housed under standard SPF conditions. Mice were bred as previously described (Gomez-Pastor et al. 2017) to generate the following genotypes WT (CK2α′$^{(+/+)}$ HTT$^{(0/0)}$), CK2α′$^{(+/-)}$ (CK2α′$^{(+/-)}$ HTT$^{(0/0)}$), zQ175 (CK2α′$^{(+/+)}$ HTT$^{(Tg/0)}$), zQ175;CK2α′$^{(+/-)}$ (CK2α′$^{(+/-)}$ HTT$^{(Tg/0)}$). Animals were analyzed at 3, 6, 12, and 22 months of age. Sample size was set to a minimum of three animals per genotype for every analysis. When possible at least two females and two males were used for each genotype and age. Littermates of the same sex were randomly assigned to experimental groups. All animal care and sacrifice procedures were approved by the University of Minnesota Institutional Animal Care and Use Committee (IACUC) in compliance with the National Institutes of Health guidelines for the care and use of laboratory animals under the approved animal protocol 1708-35063A.

## METHOD DETAILS

### siRNA transfection

For CK2α' knock-down, ST*Hdh* cells were transfected with FlexiTube siRNA (5 nmol) from Qiagen (Mm_Csnk2a2; SI00961051; SI00961058; SI00961065; SI00961072) using DharmaFECT1 per manufacturer's guidelines. As a negative control, ON-TARGETplus control Non-targeting pool siRNA (Dharmacon) was used. Cells were

collected 24 h after transfection for RNA extraction and RT-qPCR. All siRNAs have been validated by RT-qPCR and immunoblotting for knockdown efficiency of target gene.

**RNA preparation and RT-qPCR**

RNA was extracted from STHdh cells and mouse striatal tissues by using the RNeasy extraction kit (Qiagen) according to the manufacturer's instructions. cDNA for all samples was prepared from 1 µg RNA using the Superscript First Strand Synthesis System (Invitrogen) according to the manufacturer's instructions. SYBR green based PCR was performed with SYBR mix (Roche). The primer sequences for target genes were as follows; CK2α' forward: 5'- CGACTGATTGATTGGGGTCT-3' reverse: 5'-AGAATGGCTCCTTTCGGAAT-3', IL-6 forward: 5'- AGTTGCCTTCTTGGGACT-3' reverse: 5'-TCCACGATTTCCCAGAGAAC-3', PSD-95 (Dlg4) forward: 5'-CCGACAAGTTTGGATCCTGT-3', reverse: 5'-ACGGATGAAGATGGCGATAG, Drd1 forward: 5'-AAGATGCCGAGGATGACAAC-3', reverse:5'-CCCTCTCCAAAGCTGAGATG-3', Drd2 forward: 5'-TATGCCCTGGGTCGTCTATC-3', reverse: 5'-AGGACAGGACCCAGACAATG-3', Darpp32(PPP1R1B) forward: 5'-CCACCCAAAGTCGAAGAGAC-3', reverse: 5'-GCTAATGGTCTGCAGGTGCT-3', GAPDH (used as an internal control gene) forward: 5'-ACACATTGGGGGTAGGAACA-3' reverse: 5'-AACTTTGGCATTGTGGAAGG-3'. The qPCR amplification was performed using the LightCycler 480 System (Roche). Each sample was tested in triplicate and normalized to GAPDH levels. For analysis, $2^{\Delta\Delta Ct}$ method was used to calculate the relative fold gene expression of samples.

## Immunoblot analysis

Sample preparation and immunoblotting condition were performed as previously described (Gomez-Pastor et al. 2017). Striatum protein extracts from one hemisphere of mice were prepared in cell lysis buffer (25 mM Tris pH 7.4, 150 mM NaCl, 1 mM EDTA, 1% Triton-X100 and 0.1% SDS). Extra SDS was added to the suspension to a final concentration of 2% (w per v) and lysates heated at 95°C for 5 min to solubilize tissue. Total tissue homogenate was then centrifuged at 12,000 r.p.m. for 10 min. Protein samples were separated on 4–20% SDS Criterion TGX Stain-Free gels (BioRad) at 110 V. Proteins were transferred to a nitrocellulose membrane (BioRad 0.2 µm) and blocked with 5% non-fat dry milk in TBS containing 0.25% Tween-20 (TBST) for 1 h at room temperature. Primary antibodies were anti-CK2α' (Rabbit, Novus NB100-379 and Proteintech 10606-1-AP, both 1:1000), anti-Iba1 (Rabbit, FUJIFILM Wako 019-19741, 1:1000), α-syn (Mouse, Biolegend 834303, 1:1000), pS129-α-syn (Mouse, Millipore MABN826, 1:500), GAPDH (Mouse, Santacruz sc-365062, 1:10000). Quantitative analyses were performed using ImageJ software and normalized to GAPDH controls.

## Immunohistochemistry

Mice were anesthetized with Avertin (250 mg/kg Tribromoethanol) and perfused intracardially with tris-buffered saline (TBS) (25mM Tris-base, 135mM Nacl, 3mM KCl, pH 7.6) supplemented with 7.5 mM heparin. Brains were dissected, fixed with 4% PFA

in TBS at 4°C for 4-5 days, cryoprotected with 30% sucrose in TBS for 4-5 days and embedded in a 2:1 mixture of 30% sucrose in TBS:OCT (Tissue-Tek), as previously described (Gomez-Pastor et al. 2017). Brains were cryo-sectioned at 16 µm-thick coronally, washed and permeabilized in TBS with 0.2% Triton X-100 (TBST). Sections were blocked in 5% normal goat serum (NGS) in TBST for 1 h at room temperature. Primary antibodies were incubated overnight at 4°C in TBST containing 5% NGS. Secondary Alexa-fluorophore- conjugated antibodies (Invitrogen) were added (1:200 in TBST with 5% NGS) for 1-2 h at room temperature. Slides were mounted in ProLong Gold Antifade with DAPI (Invitrogen), and fluorescent images acquired on an epi-fluorescent microscope (Echo Revolve) or confocal microscope (Olympus FV1000). Primary antibodies used and dilutions are as follows: α-syn (Mouse, Biolegend 834303, 1:1000), pS129-α-syn (Mouse, Millipore MABN826, 1:500), CK2α' (Rabbit, Proteintech 10606-1-AP, 1:500), Ctip2 (Rat, Abcam ab18465, 1:500), C3d (Goat, R&D Systems AF2655, 1:200), glutamine synthetase GS (Mouse, BD Biosciences 610517, 1:1000), HTT (Mouse, Millipore, mEM48 Mab5374, 1:100), HTT (Rabbit, Abcam ab109115, 1:500), Iba1 (Rabbit, FUJIFILM Wako 019-19741, 1:200), NeuN (Mouse, Millipore MAB377, 1:1000). For cell number (Ctip, GS, NeuN, Iba1, DAPI) the Cell counter plugin from ImageJ software was used. HTT aggregates were counted manually using annotations in the Echo Revolve software and validated using the Puncta Analyzer plugin in ImageJ.

**Cytokine and chemokine array**

The Proteome Profiler Mouse Cytokine Array Panel (ARY006, R&D Systems) was used to detect the levels of cytokine/chemokine of the mouse brain as per manufacturer's instructions. Briefly, the striatum from each genotype of mice at the age of 12 - 14 months was harvested and frozen in liquid N2. Samples were then homogenized in PBS containing Halt protease inhibitor cocktail and phosphatase inhibitors (Fisher Scientific) and 1% triton X-100 (Sigma). Samples were stored at -80°C for 15 min, thawed and centrifuged at 10,000 × g for 5 min to remove cell debris. Final protein concentration was measured using BCA protein assay kit (Pierce). A total of n=6 WT, n=6 zQ175 and n=6 zQ175:CK2α'$^{(+/-)}$ mice were analyzed. Samples were grouped in three different pools for each genotype: pools 1 and 2 contained three different mice per genotype, pool 3 contained a randomized selection of 3 mice/genotype out the n=6 mice cohort. Similar numbers of male and female mice were evaluated. Protein samples were then added to the membrane and incubated with an antibody cocktail overnight at 4°C following manufacturer's instructions. Membranes were then developed using streptavidin-HRP and supersignal chemiluminescent detection (ThermoFisher). Data was analyzed using ImageJ software and presented as an average signal of three independent pool assays, calculating pairs of duplicate spots corresponding to 40 different cytokines or chemokines.

## Electrophysiological analyses

Acute dorsolateral striatum coronal slices (350 µm thick) were obtained from approximately 12 months old mice using a vibratome, as previously described (Cavaccini

et al. 2020, Teravskis et al. 2018). Researchers were blind to the mouse genotype. Briefly, the brain was quickly removed after decapitation and placed in ice-cold artificial cerebrospinal fluid (ACSF). Slices were incubated for at least 1h before use in a chamber at room temperature (21–24 ºC) in ACSF containing (in mM): NaCl 124, KCl 2.69, $KH_2PO_4$ 1.25, $MgSO_4$ 2, $NaHCO_3$ 26, $CaCl_2$ 2, ascorbic acid 0.4, and glucose 10, and continuously bubbled with carbogen (95% $O_2$ and 5% $CO_2$) (pH 7.4). Slices were then transferred to an immersion recording chamber and superfused at 2 mL/min with gassed ACSF at 30-32 ºC, and visualized under an Olympus BX50WI microscope (Olympus Optical; Japan). To study excitatory postsynaptic currents (EPSCs) picrotoxin (50 µM) and CGP54626 (1 µM) were added to the solution to block the $GABA_A$ and $GABA_B$ receptors, respectively. Whole-cell electrophysiological recordings were obtained from medium spiny neurons (MSNs) using patch electrodes (3–10 MΩ) filled with an internal solution containing in mM: $KMeSO_4$ 135, KCl 10, HEPES-K 10, NaCl 5, ATP-Mg 2.5, GTP-Na 0.3 (pH 7.3). Recordings were obtained with a PC-ONE amplifer (Dagan Instruments; Minneapolis, MN, USA). Membrane potentials were held at −70 mV. Signals were filtered at 1 kHz, acquired at a 10 kHz sampling rate, and fed to a Digidata 1440A digitizer (Molecular Devices; San Jose, CA, USA). pCLAMP 10.4 (Axon Instruments, Molecular Devices; San Jose, CA, USA) was used for stimulus generation, data display, data acquisition, and data storage. To record evoked EPSCs, theta capillaries filled with ACSF were used for bipolar stimulation and placed in the vicinity of the cell patched in the dorsolateral striatum. *Input–output curves* of EPSCs were made by increasing stimulus intensities from 0 to 100 µA. Paired-pulse facilitation was done by applying paired pulses (2 ms duration) with 25, 50, 75, 100, 200, 300, and 500 ms inter-pulse intervals. The paired-pulse ratio was calculated

by dividing the amplitude of the second EPSC by the first (PPR=EPSC-2/EPSC-1). Synaptic fatigue was assessed by applying 30 consecutive stimuli in 15 ms intervals. For *miniature EPSCs* (mEPSCs) tetrodotoxin (TTX; 1 µM) was added to the solution.

**Magnetic resonance imaging and spectroscopy**

*Animal Preparation for MR Scanning*; Researchers were blinded to the genotype of the mice during testing. Animals were induced with 3% isoflurane in a 1:1 mixture of $O_2$:$N_2O$. Mice were secured in a custom-built mouse holder and physiological status was monitored (SA Instruments) and recorded. Anesthesia was maintained with 1.5-2% isoflurane to achieve a respiration rate of 70-100 breaths per minute. Body temperature was maintained at 36-37ºC with a circulating warm water system and a heating fan controlled by feedback received from a fiber-optic rectal thermometer. The scan session was approximately 50 minutes for each animal. *MR Protocol;* All experiments were performed on a 9.4T/31 cm scanner (Agilent), as described previously(Öz et al. 2015, Friedrich et al. 2018). A quadrature surface radio frequency (RF) coil with two geometrically decoupled single turn coils (14 mm diameter) was used as the MR transceiver. Following positioning of the mouse in the magnet, coronal and sagittal multislice images were obtained using a rapid acquisition with relaxation enhancement (RARE) sequence [repetition time (TR)= 4 s, echo train length= 8, echo time (TE)= 60 ms, slice thickness= 1 mm, 7 slices] (Hennig, Nauerth, and Friedburg 1986). The volume of interest (VOI) studied was centered on the striatum (8.2 µl, 1.7 x 2.0 x 2.4 $mm^3$). All first- and second-order shims were adjusted using FASTMAP with echo-planar

readout(Gruetter and Tkác 2000). Localized $^{1}$H MR spectra were acquired with a short-echo localization by adiabatic selective refocusing (LASER) sequence [TE= 15 ms, TR= 5 s, 256 transients](Garwood and DelaBarre 2001) combined with VAPOR (variable power RF pulses with optimized relaxation delays) water suppression(Tkác et al. 1999). Spectra were saved as single scans. Unsuppressed water spectra were acquired from the same VOI for metabolite quantification. *Metabolite quantification*; Single shots were eddy current, frequency, and phase corrected using MRspa software (HTTp://www.cmrr.umn.edu/downloads/mrspa/) before averaging. The contributions of individual metabolites to the averaged spectra were quantified using LCModel(Provencher 1993) as described previously(Friedrich et al. 2018). The following metabolites were included in the basis set: alanine (Ala), ascorbate/vitamin C (Asc), aspartate (Asp), glycerophosphocholine (GPC), phosphocholine (PCho), creatine (Cr), phosphocreatine (PCr), gamma-aminobutyric acid (GABA), glucose (Glc), glutamine (Gln), glutamate (Glu), glutathione (GSH), glycine (Gly), *myo*-inositol (Ins), lactate (Lac), *N*-acetylaspartate (NAA), *N*-acetylaspartylglutamate (NAAG), phosphoethanolamine (PE), *scyllo*-inositol (Scyllo), taurine (Tau), and macromolecules (MM). The MM spectra were experimentally obtained from a VOI that covered the striatum using an inversion recovery technique [VOI = 4.7 x 2.1 x 2.7 mm$^3$, TE = 15 ms, TR = 2 s, inversion time (TIR) = 675 ms, 400 transients, N = 2]. The model metabolite spectra were generated using density matrix simulations(Deelchand et al. 2012) with the MATLAB software (MathWorks) based on previously reported chemical shifts and coupling constants(Govindaraju, Young, and Maudsley 2000). Concentrations with mean Cramér-Rao lower bounds ≤20% in any of the 3 groups were reported(Friedrich et al. 2018). If the

correlation between two metabolites was consistently high (correlation coefficient r <−0.7), their sum was reported rather than the individual values(Friedrich et al. 2018). Strong negative correlation was found in two cases, so that Cr and PCr (denoted tCr for total creatine) and GPC and PCho (denoted tCho for total choline) were reported.

**Measurement of striatal volume**

For volumetric analysis of striatum, coronal RARE images were used. The images had an in-plane resolution of 0.125 mm x 0.125 mm and 1 mm slice thickness. All volumetric quantifications were performed using ImageJ. The perimeter of the striatum was traced using a polygon selection tool and the volume measurement was performed by running Measure Stack plugin on ImageJ. All quantitative analyses were conducted blindly with respect to mouse genotype.

**Behavioral assays**

Researchers at the Mouse Behavioral core at University of Minnesota were blind to the genotypes of the mice during testing. Mice were transported from their colony room in their home cages to the behavioral testing room, where they were allowed to acclimate for at least one hour prior to the beginning of the experiment.

*Barnes Maze***:** The Barnes maze is a dry-land maze test for spatial learning and memory. It consists of a circular platform with 20 holes along the perimeter (San Diego Instruments). Spatial cues were placed on all four walls of the behavioral testing room, lit to 300 lx during testing. Mice were acclimatized to the testing room for 30 min at the

beginning of each training session. Training days consisted of 4 trials per day for 4 days. Training trials ended when the subject climbed into the escape box within the goal quadrant located under 1 of the holes or when the maximum trial duration of 180 s was reached. Subjects were run in small groups of six mice or less, so that no more than 20 min passed between trials for a given animal during training. On the day following the last training trial, memory was assessed in single 90 s probe trial tests, where the target escape box in the goal quadrant was replaced with a false box cover identical to the other 19 holes, and the exploration pattern of each subject was examined.

*Barnes Maze Reversal*: The Barnes Maze Reversal was conducted in the same way as Barnes Maze as described above besides two differences: Test consisted of 2 training days as opposed to 4 in the Barnes Maze, and the escape hole was located on the opposite side of the maze.

*Beam Walk*: The deficits of motor coordination were assessed by a beam walking test which measures a mouse's ability to maintain balance while traversing a narrow beam to reach a safe platform. For this, 19-mm (medium-round) or 10-mm (small-round) diameter and 16-mm (medium-Square) or 10-mm (small-Square) width of 3 feet long wood beams (made in house) were used and placed 19 inches above the test bench by metal supports. Each mouse was placed on the beam at one end and allowed to walk to the goal box. Foot slips were recorded manually when the hind paws slipped off the beam. Testing included 3 training days with 4 consecutive trials. The performance was measured by recording the time of traversing the beam and the number of paws faults or slips from the beam. Maximum length of time per trial was 60 s; Trials that exceeded 60 s (e.g. a mouse failed to cross the finish line within a minute) were recorded as 60 s.

*Cylinder Test*: Mice were placed in a transparent glass cylinder (40 cm length and 20 cm in diameter, made in house). The number of forelimb contacts while rearing against the wall of the cylinder was scored manually for 5 mins to examine asymmetric motor impairments.

*Delay Fear Conditioning*: The test was conducted in a chamber (Interior: 23.5"x 28"x 12.5", Exterior: 25"x 29.5”x14") equipped with a speaker and a stainless-steel foot shock grid floor (Med Associates Inc.). On Day 1, mice were trained on a 9-min training session in a testing chamber. Then, animals received 5 paired light (15-20 lx) and tone cues (8000Hz, 80 dB; Rise/fall 10ms) immediately followed by a foot shock (0.7 mA), with 60 second-intertrial intervals. Mice were then removed from the chamber and returned to its home cage. 24 h after training (Day 2), mice were re-exposed to the test chamber (no cue presentation) for 3 mins and context-dependent freezing was recorded for baseline freezing measurement. Then, mice spent 6 mins in a test chamber which presents paired light and tone cues in the last 2 mins of testing to induce cued freezing. Data collection and analysis were semi-automated via video-monitoring fear-conditioning apparatus (Med Associates, Inc.).

***Open Field Test*:** The pattern of exploration is used as a measure of anxiety-like behavior. Activity chambers (20”x20”x10”, made in house) were equipped with light intensity of 250 lx. Mice were placed in the center of the chamber and their behavior was recorded using ANY-maze software for 30 mins. The test arena was divided into a center and periphery zone. The periphery was a ~3.5-inch-wide zone adjacent to the walls and was used to determine thigmotactic behavior. Analyses were performed on

the following five measures: total locomotion (distance traveled), locomotion in the inner or outer zone, and velocity in the light phase of the cycle.

*Rotarod*: It is a standard test of motor coordination and balance in rodents. Mice were tested over 3 consecutive days. Each daily session included a single training trial of 15 min at 5 RPM on the rotarod apparatus (Ugo Basile). On day 3, the animals were tested for 3 consecutive accelerating trials of 5 min with the rotarod speed changing from 5 to 50 RPM over 300 s, with an inter-trial interval of at least 15 min. The latency to fall from the rod was recorded for each trial, with mice remaining on the rod for more than 300 sec removed and scored at 300 s.

*Y-Maze*: This test evaluated short-term spatial and working memory on a Y-maze apparatus (made in house) with three arms (15.75” × 3.5” × 7.25”) at a 120 ° angle. Animals were first moved to a testing room and habituated for 15-30 mins while setting up the apparatus. To measure spatial short-term memory, one of the three arms of the maze (“Novel Arm”) was blocked and the mouse was placed in the start arm, allowed to explore the other two arms for 10 mins while the time spent in each zone was recorded. Then, the mouse was transferred to its cage for 60-min of inter-trial interval before the test trial. Mice were then returned to the initial arm and allowed to wander around all three arms of the maze for 5 mins. Time spent in each arm and the number of entries into each arm were recorded. Spontaneous alternation task was used to assess spatial working memory and was performed at least 20 hours after the spatial memory task. In this task, the innate response of a mouse to a new environment was evaluated. Alternation was defined as entry into all three arms, e.g., ABC, BCA, or CAB, but not CAC. The mouse was habituated in the testing room for 15-20 mins while setting up the

apparatus. The animal was then placed in one arm of the maze and was allowed to move freely all three arms for 5 minutes. Latency to exit the start arm, the number and pattern of arm choices were recorded.

**Measurement of striatal volume**

For volumetric analysis of striatum, images obtained from the MRS scanning were used. The images were a series of coronal sections spaced 1 mm apart throughout the striatum with an isotropic resolution of 0.125 mm x 0.125 mm x 1 mm. All volumetric quantifications were performed using ImageJ. The serial sections were created to image stacks. The perimeter of the striatum was traced using a polygon selection tool and the volume measurement was performed by running Measure Stack plugin on ImageJ. All quantitative analyses were conducted blindly with respect to mouse genotype.

**RNA-Seq Analyses**

Gene expression analysis was carried out using the CHURP pipeline (HTTps://doi.org/10.1145/3332186.3333156). Read quality was assessed using FastQC (HTTp://www.bioinformatics.bbsrc.ac.uk/projects/fastqc). Raw reads were then trimmed to remove low quality 3' ends and adaptor contamination using Trimmomatic with the following parameter: ILLUMINACLIP:all_illumina_adapters.fa:4:15:7:2:true LEADING:3 TRAILING:3 SLIDINGWINDOW:4:15 MINLEN:18 (Bolger, Lohse, and Usadel 2014). Processed reads were aligned to mouse reference genome GRCm38 via HiSat2 (PMID: 31375807) using default parameters. Post-alignment cleaning removed duplicated

mapping, unmapped reads and reads with MAPQ<60. Gene-level expressions were quantified using Subread (PMID: 24227677), and differential gene expression was determined with DESeq2 using default setting (PMID: 25516281). Genes with a $q < 0.1$ were considered significant. Pathway and clustering analysis were completed with Ingenuity Pathway Analysis (Ingenuity Systems: RRID: SCR_008653) and gProfiler2 (PMID: 31066453). Data visualization was done using various R graphic packages, including ggplo2, ggraph and DESeq2 visualization functions.

## WGCNA Analysis

Genes with less than 10 counts in more than 90% of samples were removed from WGCNA analysis (Langfelder and Horvath 2008). The count-based gene expressions were first transformed using variance stabilizing method via DESeq2 vst function. The WGCNA R package (v1.69) was used to construct an unsigned gene co-expression network with a soft threshold power [beta] of 6. Nineteen tightly connected modules were detected, while genes that are not connected to the 19 modules are collected in the 20$^{th}$ "grey" module. WGCNA defines the expression of a given module by averaging module gene expressions, which is also called module eigengene expression. Using non-parametric Kruskal-Wallis test (p value < 0.05), we can identify modules that differ significantly among mice samples with different genotypes. For example, the "Greenyellow" module differs significantly between zQ175 mice and zQ175:CK2α'$^{(+/-)}$ mice. Data for Greenyellow module was exported using Cytoscape format for visualization. Network figures are limited to the top 10% of genes with the strongest

network connections (the topological overlap threshold was raised until only 10% of genes remained). The network modules are color coded by the differential expression between zQ175 mice and zQ175:CK2α'$^{(+/-)}$ mice: blue, downregulated in zQ175 compared to ZQ175:CK2α'$^{(+/-)}$ mice; red, upregulated in zQ175 compared to ZQ175:CK2α'$^{(+/-)}$. The size of the circles is scaled by the absolute value of the mean log2 fold change between zQ175 and ZQ175:CK2α'$^{(+/-)}$ mice.

## QUANTIFICATION AND STATISTICAL ANALYSIS

Data are expressed as Mean ± SEM, Mean ± SD or percentage, analyzed for statistical significance, and displayed by Prism 8 software (GraphPad, San Diego, CA) or Excel software (Microsoft). Pearson correlation tests were applied to test the normal distribution of experimental data. Normal distributions were compared with t-test (two-tailed) or ANOVA with appropriate post-hoc tests (Sidak's, Dunn's or Tukey's) for multiple comparisons. Non-normal distributions were compared with the non-parametric Kruskal-Wallis test with appropriate post-hoc test, as indicated. The accepted level of significance was $p \leq 0.05$, therefore samples indicated as n.s (no significant) did not reach $p \leq 0.05$. Statistical analyses for electrophysiological experiments were performed with SigmaPlot 13.0 software. No statistical methods were used to predetermine sample sizes, but sample sizes were chosen to be similar to those reported in previous publications (Gomez-Pastor et al. 2017). In the figures, we show the mean as an estimator of central tendency also when we have used a non-parametric test, for consistency with other figures in the paper and because it is more intuitive to compare the mean values.

## Acknowledgements

We are grateful to Dr. Sylvain Lesne for sharing his expertise on alpha-synuclein and sharing antibodies, Maha Syed for technical assistance, Jason Mitchell for assistance with confocal microscopy.

## Authors' contributions

RGP obtained funding for the study and designed the experiments. DY, NZ, FC, JY, TB, AT, RM, KJ, CN, TSM, SL, KG and MB performed the experiments. DY, NZ, RM, SL, KG, CN and RGP prepared and analyzed the data. GO supervised the MR data acquisition and analysis. MB supervised mouse behavioral data acquisition and analysis. RGP wrote the first draft of the manuscript and DY and NZ edited subsequent versions to which all authors contributed. All authors read and approved the final version of the manuscript.

## Funding

This work was supported by R.G.P's startup funds from University of Minnesota, the Biomedical Research Awards for Interdisciplinary New Science BRAINS (to R.G.P) and the National Institute of Health NINDS (R01 NS110694-01A1) (to R.G.P). The Center for Magnetic Resonance Research is supported by the National Institute of Biomedical Imaging and Bioengineering (NIBIB) grant P41 EB027061, the Institutional Center

Cores for Advanced Neuroimaging award P30 NS076408 and the W.M. Keck Foundation. FC received the mobility scholarship program Global Links: an Opportunity to Build a University Strategy A.A. 2018/2019 (GLOBUS Placement), Università degli Studi di Cagliari, funded through the Regione Autonoma della Sardegna. National Institute of Health NINDS (R01 NS197387) (to M.C.) and National Institute of Health NINDS R01 MH119355 and R01 NS108686 (to A.A).

## Declaration of interest

The authors declare no competing interests.

## References

1993. "A novel gene containing a trinucleotide repeat that is expanded and unstable on Huntington's disease chromosomes. The Huntington's Disease Collaborative Research Group." *Cell* 72 (6):971-983.

Al-Dalahmah, O., A. A. Sosunov, A. Shaik, K. Ofori, Y. Liu, J. P. Vonsattel, I. Adorjan, V. Menon, and J. E. Goldman. 2020. "Single-nucleus RNA-seq identifies Huntington disease astrocyte states." *Acta Neuropathol Commun* 8 (1):19. doi: 10.1186/s40478-020-0880-6.

Anderson, J. P., D. E. Walker, J. M. Goldstein, R. de Laat, K. Banducci, R. J. Caccavello, R. Barbour, J. Huang, K. Kling, M. Lee, L. Diep, P. S. Keim, X. Shen, T. Chataway, M. G. Schlossmacher, P. Seubert, D. Schenk, S. Sinha, W. P. Gai, and T. J.

1405 Chilcote. 2006. "Phosphorylation of Ser-129 is the dominant pathological modification of
1406 alpha-synuclein in familial and sporadic Lewy body disease." *J Biol Chem* 281
1407 (40):29739-52. doi: 10.1074/jbc.M600933200.

1408 Anderson, M. A., Y. Ao, and M. V. Sofroniew. 2014. "Heterogeneity of reactive
1409 astrocytes." *Neurosci Lett* 565:23-9. doi: 10.1016/j.neulet.2013.12.030.

1410 Araque, A., R. P. Sanzgiri, V. Parpura, and P. G. Haydon. 1999. "Astrocyte-induced
1411 modulation of synaptic transmission." *Can J Physiol Pharmacol* 77 (9):699-706.

1412 Arlotta, P., B. J. Molyneaux, D. Jabaudon, Y. Yoshida, and J. D. Macklis. 2008. "Ctip2
1413 controls the differentiation of medium spiny neurons and the establishment of the
1414 cellular architecture of the striatum." *J Neurosci* 28 (3):622-32. doi:
1415 10.1523/JNEUROSCI.2986-07.2008.

1416 Atwal, R. S., C. R. Desmond, N. Caron, T. Maiuri, J. Xia, S. Sipione, and R. Truant.
1417 2011. "Kinase inhibitors modulate huntingtin cell localization and toxicity."
1418 *Nat.Chem.Biol.* 7 (7):453-460.

1419 Bender, M., L. Schwind, D. Grundmann, M. Martin, M. Klotz, C. Götz, M. Montenarh,
1420 and K. H. Schäfer. 2017. "Impact of protein kinase CK2 inhibitors on proliferation and
1421 differentiation of neural stem cells." *Heliyon* 3 (6):e00318. doi:
1422 10.1016/j.heliyon.2017.e00318.

1423 Bian, Y., M. Ye, C. Wang, K. Cheng, C. Song, M. Dong, Y. Pan, H. Qin, and H. Zou.
1424 2013. "Global screening of CK2 kinase substrates by an integrated phosphoproteomics
1425 workflow." *Sci.Rep.* 3:3460.

1426 Björkqvist, M., E. J. Wild, J. Thiele, A. Silvestroni, R. Andre, N. Lahiri, E. Raibon, R. V.
1427 Lee, C. L. Benn, D. Soulet, A. Magnusson, B. Woodman, C. Landles, M. A. Pouladi, M.
1428 R. Hayden, A. Khalili-Shirazi, M. W. Lowdell, P. Brundin, G. P. Bates, B. R. Leavitt, T.
1429 Möller, and S. J. Tabrizi. 2008. "A novel pathogenic pathway of immune activation
1430 detectable before clinical onset in Huntington's disease." *J Exp Med* 205 (8):1869-77.
1431 doi: 10.1084/jem.20080178.

1432 Bolger, A. M., M. Lohse, and B. Usadel. 2014. "Trimmomatic: a flexible trimmer for
1433 Illumina sequence data." *Bioinformatics* 30 (15):2114-20. doi:
1434 10.1093/bioinformatics/btu170.

1435 Brand, A., C. Richter-Landsberg, and D. Leibfritz. 1993. "Multinuclear NMR studies on
1436 the energy metabolism of glial and neuronal cells." *Dev Neurosci* 15 (3-5):289-98. doi:
1437 10.1159/000111347.

1438 Breza, M., E. Emmanouilidou, E. Leandrou, C. Kartanou, A. Bougea, M. Panas, L.
1439 Stefanis, G. Karadima, K. Vekrellis, and G. Koutsis. 2020. "Elevated Serum α-Synuclein
1440 Levels in Huntington's Disease Patients." *Neuroscience* 431:34-39. doi:
1441 10.1016/j.neuroscience.2020.01.037.

1442 Castello, J., A. Ragnauth, E. Friedman, and H. Rebholz. 2017. "CK2-An Emerging
1443 Target for Neurological and Psychiatric Disorders." *Pharmaceuticals (Basel)* 10 (1). doi:
1444 10.3390/ph10010007.

1445 Castillo, M., L. Kwock, J. Scatliff, and S. K. Mukherji. 1998. "Proton MR spectroscopy in
1446 neoplastic and non-neoplastic brain disorders." *Magn Reson Imaging Clin N Am* 6
1447 (1):1-20.

1448 Cavaccini, A., C. Durkee, P. Kofuji, R. Tonini, and A. Araque. 2020. "Astrocyte Signaling
1449 Gates Long-Term Depression at Corticostriatal Synapses of the Direct Pathway." *J*
1450 *Neurosci* 40 (30):5757-5768. doi: 10.1523/JNEUROSCI.2369-19.2020.

1451 Ceglia, I., M. Flajolet, and H. Rebholz. 2011. "Predominance of CK2α over CK2α' in the
1452 mammalian brain." *Mol Cell Biochem* 356 (1-2):169-75. doi: 10.1007/s11010-011-0963-
1453 6.

1454 Chang, K. H., Y. R. Wu, Y. C. Chen, and C. M. Chen. 2015. "Plasma inflammatory
1455 biomarkers for Huntington's disease patients and mouse model." *Brain Behav Immun*
1456 44:121-7. doi: 10.1016/j.bbi.2014.09.011.

1457 Chung, C. Y., J. B. Koprich, H. Siddiqi, and O. Isacson. 2009. "Dynamic changes in
1458 presynaptic and axonal transport proteins combined with striatal neuroinflammation
1459 precede dopaminergic neuronal loss in a rat model of AAV alpha-synucleinopathy." *J*
1460 *Neurosci* 29 (11):3365-73. doi: 10.1523/JNEUROSCI.5427-08.2009.

1461 Clarke, L. E., S. A. Liddelow, C. Chakraborty, A. E. Münch, M. Heiman, and B. A.
1462 Barres. 2018. "Normal aging induces A1-like astrocyte reactivity." *Proc Natl Acad Sci U*
1463 *S A* 115 (8):E1896-E1905. doi: 10.1073/pnas.1800165115.

1464 Consortium, Genetic Modifiers of Huntington's Disease (GeM-HD). 2015. "Identification
1465 of Genetic Factors that Modify Clinical Onset of Huntington's Disease." *Cell* 162
1466 (3):516-26. doi: 10.1016/j.cell.2015.07.003.

1467 Crotti, A., and C. K. Glass. 2015. "The choreography of neuroinflammation in
1468 Huntington's disease." *Trends Immunol* 36 (6):364-73. doi: 10.1016/j.it.2015.04.007.

1469 Curtin, P. C., A. M. Farrar, S. Oakeshott, J. Sutphen, J. Berger, M. Mazzella, K. Cox, D.
1470 He, W. Alosio, L. C. Park, D. Howland, and D. Brunner. 2015. "Cognitive Training at a
1471 Young Age Attenuates Deficits in the zQ175 Mouse Model of HD." *Front Behav*
1472 *Neurosci* 9:361. doi: 10.3389/fnbeh.2015.00361.

1473 Davidi, D., M. Schechter, S. A. Elhadi, A. Matatov, L. Nathanson, and R. Sharon. 2020.
1474 "α-Synuclein Translocates to the Nucleus to Activate Retinoic-Acid-Dependent Gene
1475 Transcription." *iScience* 23 (3):100910. doi: 10.1016/j.isci.2020.100910.

1476 Decressac, M., B. Kadkhodaei, B. Mattsson, A. Laguna, T. Perlmann, and A. Björklund.
1477 2012. "α-Synuclein-induced down-regulation of Nurr1 disrupts GDNF signaling in nigral
1478 dopamine neurons." *Sci Transl Med* 4 (163):163ra156. doi:
1479 10.1126/scitranslmed.3004676.

1480 Deelchand, D. K., P. G. Henry, K. Uğurbil, and M. Marjańska. 2012. "Measurement of
1481 transverse relaxation times of J-coupled metabolites in the human visual cortex at 4 T."
1482 *Magn Reson Med* 67 (4):891-7. doi: 10.1002/mrm.23080.

1483 Deng, Y. P., T. Wong, J. Y. Wan, and A. Reiner. 2014. "Differential loss of
1484 thalamostriatal and corticostriatal input to striatal projection neuron types prior to overt

1485 motor symptoms in the Q140 knock-in mouse model of Huntington's disease." *Front*
1486 *Syst Neurosci* 8:198. doi: 10.3389/fnsys.2014.00198.

1487 Diaz-Castro, B., M. R. Gangwani, X. Yu, G. Coppola, and B. S. Khakh. 2019. "Astrocyte
1488 molecular signatures in Huntington's disease." *Sci Transl Med* 11 (514). doi:
1489 10.1126/scitranslmed.aaw8546.

1490 DiFiglia, M., E. Sapp, K. O. Chase, S. W. Davies, G. P. Bates, J. P. Vonsattel, and N.
1491 Aronin. 1997. "Aggregation of huntingtin in neuronal intranuclear inclusions and
1492 dystrophic neurites in brain." *Science* 277 (5334):1990-3.

1493 Eroglu, C., and B. A. Barres. 2010. "Regulation of synaptic connectivity by glia." *Nature*
1494 468 (7321):223-31. doi: 10.1038/nature09612.

1495 Fan, M. M., H. Zhang, M. R. Hayden, S. L. Pelech, and L. A. Raymond. 2008a.
1496 "Protective up-regulation of CK2 by mutant huntingtin in cells co-expressing NMDA
1497 receptors." *J Neurochem* 104 (3):790-805. doi: 10.1111/j.1471-4159.2007.05016.x.

1498 Fan, M. M., H. Zhang, M. R. Hayden, S. L. Pelech, and L. A. Raymond. 2008b.
1499 "Protective up-regulation of CK2 by mutant huntingtin in cells co-expressing NMDA
1500 receptors." *J.Neurochem.* 104 (3):790-805.

1501 Farrar, A. M., C. A. Murphy, N. E. Paterson, S. Oakeshott, D. He, W. Alosio, K.
1502 McConnell, L. B. Menalled, S. Ramboz, L. C. Park, D. Howland, and D. Brunner. 2014.
1503 "Cognitive deficits in transgenic and knock-in HTT mice parallel those in Huntington's
1504 disease." *J Huntingtons Dis* 3 (2):145-58. doi: 10.3233/JHD-130061.

1505 Fernández-Nogales, M., J. R. Cabrera, M. Santos-Galindo, J. J. Hoozemans, I. Ferrer,
1506 A. J. Rozemuller, F. Hernández, J. Avila, and J. J. Lucas. 2014. "Huntington's disease is
1507 a four-repeat tauopathy with tau nuclear rods." *Nat Med* 20 (8):881-5. doi:
1508 10.1038/nm.3617.

1509 Ferrante, R. J., N. W. Kowall, and E. P. Richardson. 1991. "Proliferative and
1510 degenerative changes in striatal spiny neurons in Huntington's disease: a combined
1511 study using the section-Golgi method and calbindin D28k immunocytochemistry." *J*
1512 *Neurosci* 11 (12):3877-87.

1513 Fienberg, A. A., N. Hiroi, P. G. Mermelstein, W. Song, G. L. Snyder, A. Nishi, A.
1514 Cheramy, J. P. O'Callaghan, D. B. Miller, D. G. Cole, R. Corbett, C. N. Haile, D. C.
1515 Cooper, S. P. Onn, A. A. Grace, C. C. Ouimet, F. J. White, S. E. Hyman, D. J. Surmeier,
1516 J. Girault, E. J. Nestler, and P. Greengard. 1998. "DARPP-32: regulator of the efficacy
1517 of dopaminergic neurotransmission." *Science* 281 (5378):838-42. doi:
1518 10.1126/science.281.5378.838.

1519 Franchin, C., C. Borgo, L. Cesaro, S. Zaramella, J. Vilardell, M. Salvi, G. Arrigoni, and
1520 L. A. Pinna. 2018. "Re-evaluation of protein kinase CK2 pleiotropy: new insights
1521 provided by a phosphoproteomics analysis of CK2 knockout cells." *Cell Mol Life Sci* 75
1522 (11):2011-2026. doi: 10.1007/s00018-017-2705-8.

1523 Franciosi, S., J. K. Ryu, Y. Shim, A. Hill, C. Connolly, M. R. Hayden, J. G. McLarnon,
1524 and B. R. Leavitt. 2012. "Age-dependent neurovascular abnormalities and altered
1525 microglial morphology in the YAC128 mouse model of Huntington disease." *Neurobiol*
1526 *Dis* 45 (1):438-49. doi: 10.1016/j.nbd.2011.09.003.

1527 Friedrich, J., H. B. Kordasiewicz, B. O'Callaghan, H. P. Handler, C. Wagener, L. Duvick,
1528 E. E. Swayze, O. Rainwater, B. Hofstra, M. Benneyworth, T. Nichols-Meade, P. Yang,
1529 Z. Chen, J. P. Ortiz, H. B. Clark, G. Öz, S. Larson, H. Y. Zoghbi, C. Henzler, and H. T.
1530 Orr. 2018. "Antisense oligonucleotide-mediated ataxin-1 reduction prolongs survival in
1531 SCA1 mice and reveals disease-associated transcriptome profiles." *JCI Insight* 3 (21).
1532 doi: 10.1172/jci.insight.123193.

1533 Fujiwara, H., M. Hasegawa, N. Dohmae, A. Kawashima, E. Masliah, M. S. Goldberg, J.
1534 Shen, K. Takio, and T. Iwatsubo. 2002. "alpha-Synuclein is phosphorylated in
1535 synucleinopathy lesions." *Nat.Cell Biol.* 4 (2):160-164.

1536 Gallardo-Orihuela, A., I. Hervás-Corpión, C. Hierro-Bujalance, D. Sanchez-Sotano, G.
1537 Jiménez-Gómez, F. Mora-López, A. Campos-Caro, M. Garcia-Alloza, and L. M. Valor.
1538 2019. "Transcriptional correlates of the pathological phenotype in a Huntington's
1539 disease mouse model." *Sci Rep* 9 (1):18696. doi: 10.1038/s41598-019-55177-9.

1540 Garcia, V. J., D. J. Rushton, C. M. Tom, N. D. Allen, P. J. Kemp, C. N. Svendsen, and
1541 V. B. Mattis. 2019. "Huntington's Disease Patient-Derived Astrocytes Display
1542 Electrophysiological Impairments and Reduced Neuronal Support." *Front Neurosci*
1543 13:669. doi: 10.3389/fnins.2019.00669.

1544 Garwood, M., and L. DelaBarre. 2001. "The return of the frequency sweep: designing
1545 adiabatic pulses for contemporary NMR." *J Magn Reson* 153 (2):155-77. doi:
1546 10.1006/jmre.2001.2340.

1547 Glikmann-Johnston, Y., K. D. Fink, P. Deng, A. Torrest, and J. C. Stout. 2019. "Spatial
1548 memory in Huntington's disease: A comparative review of human and animal data."
1549 *Neurosci Biobehav Rev* 98:194-207. doi: 10.1016/j.neubiorev.2019.01.015.

1550 Gomez-Pastor, R., E. T. Burchfiel, D. W. Neef, A. M. Jaeger, E. Cabiscol, S. U.
1551 McKinstry, A. Doss, A. Aballay, D. C. Lo, S. S. Akimov, C. A. Ross, C. Eroglu, and D. J.
1552 Thiele. 2017. "Abnormal degradation of the neuronal stress-protective transcription
1553 factor HSF1 in Huntington's disease." *Nat Commun* 8:14405. doi:
1554 10.1038/ncomms14405.

1555 Gomez-Pastor, R., E. T. Burchfiel, and D. J. Thiele. 2017. "Regulation of heat shock
1556 transcription factors and their roles in physiology and disease." *Nat Rev Mol Cell Biol*.
1557 doi: 10.1038/nrm.2017.73.

1558 Govindaraju, V., K. Young, and A. A. Maudsley. 2000. "Proton NMR chemical shifts and
1559 coupling constants for brain metabolites." *NMR Biomed* 13 (3):129-53. doi:
1560 10.1002/1099-1492(200005)13:3<129::aid-nbm619>3.0.co;2-v.

1561 Greenwood, J. A., C. W. Scott, R. C. Spreen, C. B. Caputo, and G. V. Johnson. 1994.
1562 "Casein kinase II preferentially phosphorylates human tau isoforms containing an
1563 amino-terminal insert. Identification of threonine 39 as the primary phosphate acceptor."
1564 *J Biol Chem* 269 (6):4373-80.

1565 Gruetter, R., and I. Tkác. 2000. "Field mapping without reference scan using
1566 asymmetric echo-planar techniques." *Magn Reson Med* 43 (2):319-23. doi:
1567 10.1002/(sici)1522-2594(200002)43:2<319::aid-mrm22>3.0.co;2-1.

1568 Hara, S., S. Arawaka, H. Sato, Y. Machiya, C. Cui, A. Sasaki, S. Koyama, and T. Kato.
1569 2013. "Serine 129 phosphorylation of membrane-associated α-synuclein modulates
1570 dopamine transporter function in a G protein-coupled receptor kinase-dependent
1571 manner." *Mol Biol Cell* 24 (11):1649-60, S1-3. doi: 10.1091/mbc.E12-12-0903.

1572 Harrington, D. L., M. M. Smith, Y. Zhang, N. E. Carlozzi, J. S. Paulsen, and PREDICT-
1573 HD Investigators of the Huntington Study Group. 2012. "Cognitive domains that predict
1574 time to diagnosis in prodromal Huntington disease." *J Neurol Neurosurg Psychiatry* 83
1575 (6):612-9. doi: 10.1136/jnnp-2011-301732.

1576 Heikkinen, T., K. Lehtimäki, N. Vartiainen, J. Puoliväli, S. J. Hendricks, J. R. Glaser, A.
1577 Bradaia, K. Wadel, C. Touller, O. Kontkanen, J. M. Yrjänheikki, B. Buisson, D. Howland,
1578 V. Beaumont, I. Munoz-Sanjuan, and L. C. Park. 2012. "Characterization of
1579 neurophysiological and behavioral changes, MRI brain volumetry and 1H MRS in zQ175
1580 knock-in mouse model of Huntington's disease." *PLoS One* 7 (12):e50717. doi:
1581 10.1371/journal.pone.0050717.

1582 Hennig, J., A. Nauerth, and H. Friedburg. 1986. "RARE imaging: a fast imaging method
1583 for clinical MR." *Magn Reson Med* 3 (6):823-33. doi: 10.1002/mrm.1910030602.

1584 Hodges, A., A. D. Strand, A. K. Aragaki, A. Kuhn, T. Sengstag, G. Hughes, L. A.
1585 Elliston, C. Hartog, D. R. Goldstein, D. Thu, Z. R. Hollingsworth, F. Collin, B. Synek, P.
1586 A. Holmans, A. B. Young, N. S. Wexler, M. Delorenzi, C. Kooperberg, S. J. Augood, R.
1587 L. Faull, J. M. Olson, L. Jones, and R. Luthi-Carter. 2006. "Regional and cellular gene
1588 expression changes in human Huntington's disease brain." *Hum.Mol.Genet.* 15 (6):965-
1589 977.

1590 Hoenen, C., A. Gustin, C. Birck, M. Kirchmeyer, N. Beaume, P. Felten, L. Grandbarbe,
1591 P. Heuschling, and T. Heurtaux. 2016. "Alpha-Synuclein Proteins Promote Pro-
1592 Inflammatory Cascades in Microglia: Stronger Effects of the A53T Mutant." *PLoS One*
1593 11 (9):e0162717. doi: 10.1371/journal.pone.0162717.

1594 Hsiao, H. Y., F. L. Chiu, C. M. Chen, Y. R. Wu, H. M. Chen, Y. C. Chen, H. C. Kuo, and
1595 Y. Chern. 2014. "Inhibition of soluble tumor necrosis factor is therapeutic in Huntington's
1596 disease." *Hum Mol Genet* 23 (16):4328-44. doi: 10.1093/hmg/ddu151.

1597 Huang, T. N., and Y. P. Hsueh. 2015. "Brain-specific transcriptional regulator T-brain-1
1598 controls brain wiring and neuronal activity in autism spectrum disorders." *Front*
1599 *Neurosci* 9:406. doi: 10.3389/fnins.2015.00406.

1600 Indersmitten, T., C. H. Tran, C. T. Cepeda, and M. S. Levine. 2015. "Altered Excitatory
1601 and Inhibitory Inputs to Striatal Medium-Sized Spiny Neurons and Cortical Pyramidal
1602 Neurons in the Q175 Mouse Model of Huntington's Disease." *J.Neurophysiol.*:jn.

1603 Ising, C., C. Venegas, S. Zhang, H. Scheiblich, S. V. Schmidt, A. Vieira-Saecker, S.
1604 Schwartz, S. Albasset, R. M. McManus, D. Tejera, A. Griep, F. Santarelli, F. Brosseron,
1605 S. Opitz, J. Stunden, M. Merten, R. Kayed, D. T. Golenbock, D. Blum, E. Latz, L. Buée,
1606 and M. T. Heneka. 2019. "NLRP3 inflammasome activation drives tau pathology."
1607 *Nature* 575 (7784):669-673. doi: 10.1038/s41586-019-1769-z.

1608 Jeon, S. G., A. Yoo, D. W. Chun, S. B. Hong, H. Chung, J. I. Kim, and M. Moon. 2020.
1609 "The Critical Role of Nurr1 as a Mediator and Therapeutic Target in Alzheimer's

1610 Disease-related Pathogenesis." *Aging Dis* 11 (3):705-724. doi:
1611 10.14336/AD.2019.0718.

1612 Kato, T., M. Delhase, A. Hoffmann, and M. Karin. 2003. "CK2 Is a C-Terminal IkappaB
1613 Kinase Responsible for NF-kappaB Activation during the UV Response." *Mol Cell* 12
1614 (4):829-39. doi: 10.1016/s1097-2765(03)00358-7.

1615 Khakh, B. S., V. Beaumont, R. Cachope, I. Munoz-Sanjuan, S. A. Goldman, and R.
1616 Grantyn. 2017. "Unravelling and Exploiting Astrocyte Dysfunction in Huntington's
1617 Disease." *Trends Neurosci* 40 (7):422-437. doi: 10.1016/j.tins.2017.05.002.

1618 Kolodziejczyk, K., and L. A. Raymond. 2016. "Differential changes in thalamic and
1619 cortical excitatory synapses onto striatal spiny projection neurons in a Huntington
1620 disease mouse model." *Neurobiol Dis* 86:62-74. doi: 10.1016/j.nbd.2015.11.020.

1621 Langfelder, P., J. P. Cantle, D. Chatzopoulou, N. Wang, F. Gao, I. Al-Ramahi, X. H. Lu,
1622 E. M. Ramos, K. El-Zein, Y. Zhao, S. Deverasetty, A. Tebbe, C. Schaab, D. J. Lavery,
1623 D. Howland, S. Kwak, J. Botas, J. S. Aaronson, J. Rosinski, G. Coppola, S. Horvath,
1624 and X. W. Yang. 2016. "Integrated genomics and proteomics define huntingtin CAG
1625 length-dependent networks in mice." *Nat Neurosci* 19 (4):623-33. doi: 10.1038/nn.4256.

1626 Langfelder, P., and S. Horvath. 2008. "WGCNA: an R package for weighted correlation
1627 network analysis." *BMC Bioinformatics* 9:559. doi: 10.1186/1471-2105-9-559.

1628 Lee, G., M. Tanaka, K. Park, S. S. Lee, Y. M. Kim, E. Junn, S. H. Lee, and M. M.
1629 Mouradian. 2004. "Casein kinase II-mediated phosphorylation regulates alpha-

synuclein/synphilin-1 interaction and inclusion body formation." *J Biol Chem* 279 (8):6834-9. doi: 10.1074/jbc.M312760200.

Li, K., J. Li, J. Zheng, and S. Qin. 2019. "Reactive Astrocytes in Neurodegenerative Diseases." *Aging Dis* 10 (3):664-675. doi: 10.14336/AD.2018.0720.

Lian, H., A. Litvinchuk, A. C. Chiang, N. Aithmitti, J. L. Jankowsky, and H. Zheng. 2016. "Astrocyte-Microglia Cross Talk through Complement Activation Modulates Amyloid Pathology in Mouse Models of Alzheimer's Disease." *J Neurosci* 36 (2):577-89. doi: 10.1523/JNEUROSCI.2117-15.2016.

Liddelow, S. A., K. A. Guttenplan, L. E. Clarke, F. C. Bennett, C. J. Bohlen, L. Schirmer, M. L. Bennett, A. E. Münch, W. S. Chung, T. C. Peterson, D. K. Wilton, A. Frouin, B. A. Napier, N. Panicker, M. Kumar, M. S. Buckwalter, D. H. Rowitch, V. L. Dawson, T. M. Dawson, B. Stevens, and B. A. Barres. 2017. "Neurotoxic reactive astrocytes are induced by activated microglia." *Nature* 541 (7638):481-487. doi: 10.1038/nature21029.

Litchfield, D. W. 2003. "Protein kinase CK2: structure, regulation and role in cellular decisions of life and death." *Biochem.J.* 369 (Pt 1):1-15.

Liu, P., B. R. Smith, M. L. Montonye, L. J. Kemper, K. Leinonen-Wright, K. M. Nelson, L. Higgins, C. R. Guerrero, T. W. Markowski, X. Zhao, A. J. Petersen, D. S. Knopman, R. C. Petersen, and K. H. Ashe. 2020. "A soluble truncated tau species related to cognitive dysfunction is elevated in the brain of cognitively impaired human individuals." *Sci Rep* 10 (1):3869. doi: 10.1038/s41598-020-60777-x.

1650 Luthi-Carter, R., A. Strand, N. L. Peters, S. M. Solano, Z. R. Hollingsworth, A. S.
1651 Menon, A. S. Frey, B. S. Spektor, E. B. Penney, G. Schilling, C. A. Ross, D. R. Borchelt,
1652 S. J. Tapscott, A. B. Young, J. H. Cha, and J. M. Olson. 2000. "Decreased expression
1653 of striatal signaling genes in a mouse model of Huntington's disease." *Hum Mol Genet*
1654 9 (9):1259-71.

1655 Masliah, E., D. S. Iimoto, M. Mallory, T. Albright, L. Hansen, and T. Saitoh. 1992.
1656 "Casein kinase II alteration precedes tau accumulation in tangle formation."
1657 *Am.J.Pathol.* 140 (2):263-268.

1658 Masliah, E., E. Rockenstein, I. Veinbergs, M. Mallory, M. Hashimoto, A. Takeda, Y.
1659 Sagara, A. Sisk, and L. Mucke. 2000. "Dopaminergic loss and inclusion body formation
1660 in alpha-synuclein mice: implications for neurodegenerative disorders." *Science* 287
1661 (5456):1265-9. doi: 10.1126/science.287.5456.1265.

1662 Menalled, L. B., A. E. Kudwa, S. Miller, J. Fitzpatrick, J. Watson-Johnson, N. Keating,
1663 M. Ruiz, R. Mushlin, W. Alosio, K. McConnell, D. Connor, C. Murphy, S. Oakeshott, M.
1664 Kwan, J. Beltran, A. Ghavami, D. Brunner, L. C. Park, S. Ramboz, and D. Howland.
1665 2012a. "Comprehensive behavioral and molecular characterization of a new knock-in
1666 mouse model of Huntington's disease: zQ175." *PLoS One* 7 (12):e49838. doi:
1667 10.1371/journal.pone.0049838.

1668 Menalled, L. B., A. E. Kudwa, S. Miller, J. Fitzpatrick, J. Watson-Johnson, N. Keating,
1669 M. Ruiz, R. Mushlin, W. Alosio, K. McConnell, D. Connor, C. Murphy, S. Oakeshott, M.
1670 Kwan, J. Beltran, A. Ghavami, D. Brunner, L. C. Park, S. Ramboz, and D. Howland.

2012b. "Comprehensive behavioral and molecular characterization of a new knock-in mouse model of Huntington's disease: zQ175." *PLoS.One.* 7 (12):e49838.

Mikula, M., K. Hanusek, A. Paziewska, A. Dzwonek, T. Rubel, K. Bomsztyk, and J. Ostrowski. 2010. "Halogenated imidazole derivatives block RNA polymerase II elongation along mitogen inducible genes." *BMC Mol Biol* 11:4. doi: 10.1186/1471-2199-11-4.

Milnerwood, A. J., and L. A. Raymond. 2010. "Early synaptic pathophysiology in neurodegeneration: insights from Huntington's disease." *Trends Neurosci* 33 (11):513-23. doi: 10.1016/j.tins.2010.08.002.

Mottahedin, A., M. Ardalan, T. Chumak, I. Riebe, J. Ek, and C. Mallard. 2017. "Effect of Neuroinflammation on Synaptic Organization and Function in the Developing Brain: Implications for Neurodevelopmental and Neurodegenerative Disorders." *Front Cell Neurosci* 11:190. doi: 10.3389/fncel.2017.00190.

Niefind, K., B. Guerra, I. Ermakowa, and O. G. Issinger. 2001. "Crystal structure of human protein kinase CK2: insights into basic properties of the CK2 holoenzyme." *EMBO J.* 20 (19):5320-5331.

Olsen, B. B., B. Boldyreff, K. Niefind, and O. G. Issinger. 2006. "Purification and characterization of the CK2alpha'-based holoenzyme, an isozyme of CK2alpha: a comparative analysis." *Protein Expr.Purif.* 47 (2):651-661.

Olsen, J. V., M. Vermeulen, A. Santamaria, C. Kumar, M. L. Miller, L. J. Jensen, F. Gnad, J. Cox, T. S. Jensen, E. A. Nigg, S. Brunak, and M. Mann. 2010. "Quantitative

1692 phosphoproteomics reveals widespread full phosphorylation site occupancy during
1693 mitosis." *Sci Signal* 3 (104):ra3. doi: 10.1126/scisignal.2000475.

1694 Oueslati, A. 2016. "Implication of Alpha-Synuclein Phosphorylation at S129 in
1695 Synucleinopathies: What Have We Learned in the Last Decade?" *J Parkinsons Dis* 6
1696 (1):39-51. doi: 10.3233/JPD-160779.

1697 Paulsen, J. S. 2011. "Cognitive impairment in Huntington disease: diagnosis and
1698 treatment." *Curr Neurol Neurosci Rep* 11 (5):474-83. doi: 10.1007/s11910-011-0215-x.

1699 Pavese, N., A. Gerhard, Y. F. Tai, A. K. Ho, F. Turkheimer, R. A. Barker, D. J. Brooks,
1700 and P. Piccini. 2006. "Microglial activation correlates with severity in Huntington
1701 disease: a clinical and PET study." *Neurology* 66 (11):1638-43. doi:
1702 10.1212/01.wnl.0000222734.56412.17.

1703 Peng, Q., B. Wu, M. Jiang, J. Jin, Z. Hou, J. Zheng, J. Zhang, and W. Duan. 2016.
1704 "Characterization of Behavioral, Neuropathological, Brain Metabolic and Key Molecular
1705 Changes in zQ175 Knock-In Mouse Model of Huntington's Disease." *PLoS One* 11
1706 (2):e0148839. doi: 10.1371/journal.pone.0148839.

1707 Petkau, T. L., A. Hill, C. Connolly, G. Lu, P. Wagner, N. Kosior, J. Blanco, and B. R.
1708 Leavitt. 2019. "Mutant huntingtin expression in microglia is neither required nor sufficient
1709 to cause the Huntington's disease-like phenotype in BACHD mice." *Hum Mol Genet* 28
1710 (10):1661-1670. doi: 10.1093/hmg/ddz009.

1711 Pido-Lopez, J., B. Tanudjojo, S. Farag, M. K. Bondulich, R. Andre, S. J. Tabrizi, and G.
1712 P. Bates. 2019. "Inhibition of tumour necrosis factor alpha in the R6/2 mouse model of

1713 Huntington's disease by etanercept treatment." *Sci Rep* 9 (1):7202. doi:
1714 10.1038/s41598-019-43627-3.

1715 Piiponniemi, T. O., T. Parkkari, T. Heikkinen, J. Puoliväli, L. C. Park, R. Cachope, and
1716 M. V. Kopanitsa. 2018. "Impaired Performance of the Q175 Mouse Model of
1717 Huntington's Disease in the Touch Screen Paired Associates Learning Task." *Front*
1718 *Behav Neurosci* 12:226. doi: 10.3389/fnbeh.2018.00226.

1719 Pinna, L. A. 2002. "Protein kinase CK2: a challenge to canons." *J.Cell Sci.* 115 (Pt
1720 20):3873-3878.

1721 Provencher, S. W. 1993. "Estimation of metabolite concentrations from localized in vivo
1722 proton NMR spectra." *Magn Reson Med* 30 (6):672-9. doi: 10.1002/mrm.1910300604.

1723 Rebholz, H., M. Zhou, A. C. Nairn, P. Greengard, and M. Flajolet. 2013. "Selective
1724 knockout of the casein kinase 2 in d1 medium spiny neurons controls dopaminergic
1725 function." *Biol.Psychiatry* 74 (2):113-121.

1726 Reinhart, P. H., L. S. Kaltenbach, C. Essrich, D. E. Dunn, J. A. Eudailey, C. T.
1727 DeMarco, G. J. Turmel, J. C. Whaley, A. Wood, S. Cho, and D. C. Lo. 2011.
1728 "Identification of anti-inflammatory targets for Huntington's disease using a brain slice-
1729 based screening assay." *Neurobiol.Dis.* 43 (1):248-256.

1730 Riessland, M., A. Kaczmarek, S. Schneider, K. J. Swoboda, H. Löhr, C. Bradler, V.
1731 Grysko, M. Dimitriadi, S. Hosseinibarkooie, L. Torres-Benito, M. Peters, A. Upadhyay,
1732 N. Biglari, S. Kröber, I. Hölker, L. Garbes, C. Gilissen, A. Hoischen, G. Nürnberg, P.
1733 Nürnberg, M. Walter, F. Rigo, C. F. Bennett, M. J. Kye, A. C. Hart, M. Hammerschmidt,

1734 P. Kloppenburg, and B. Wirth. 2017. "Neurocalcin Delta Suppression Protects against
1735 Spinal Muscular Atrophy in Humans and across Species by Restoring Impaired
1736 Endocytosis." *Am J Hum Genet* 100 (2):297-315. doi: 10.1016/j.ajhg.2017.01.005.

1737 Rosenberger, A. F., T. H. Morrema, W. H. Gerritsen, E. S. van Haastert, H. Snkhchyan,
1738 R. Hilhorst, A. J. Rozemuller, P. Scheltens, der V. van, and J. J. Hoozemans. 2016.
1739 "Increased occurrence of protein kinase CK2 in astrocytes in Alzheimer's disease
1740 pathology." *J.Neuroinflammation.* 13 (1):4.

1741 Savage, J. C., M. K. St-Pierre, M. Carrier, H. El Hajj, S. W. Novak, M. G. Sanchez, F.
1742 Cicchetti, and M. Tremblay. 2020. "Microglial physiological properties and interactions
1743 with synapses are altered at presymptomatic stages in a mouse model of Huntington's
1744 disease pathology." *J Neuroinflammation* 17 (1):98. doi: 10.1186/s12974-020-01782-9.

1745 Schaser, A. J., V. R. Osterberg, S. E. Dent, T. L. Stackhouse, C. M. Wakeham, S. W.
1746 Boutros, L. J. Weston, N. Owen, T. A. Weissman, E. Luna, J. Raber, K. C. Luk, A. K.
1747 McCullough, R. L. Woltjer, and V. K. Unni. 2019. "Alpha-synuclein is a DNA binding
1748 protein that modulates DNA repair with implications for Lewy body disorders." *Sci Rep*
1749 9 (1):10919. doi: 10.1038/s41598-019-47227-z.

1750 Schell, H., T. Hasegawa, M. Neumann, and P. J. Kahle. 2009. "Nuclear and neuritic
1751 distribution of serine-129 phosphorylated alpha-synuclein in transgenic mice."
1752 *Neuroscience* 160 (4):796-804. doi: 10.1016/j.neuroscience.2009.03.002.

1753 Selmaj, K. W., M. Farooq, W. T. Norton, C. S. Raine, and C. F. Brosnan. 1990.
1754 "Proliferation of astrocytes in vitro in response to cytokines. A primary role for tumor
1755 necrosis factor." *J Immunol* 144 (1):129-35.

1756 Shalash, A., M. Salama, M. Makar, T. Roushdy, H. H. Elrassas, W. Mohamed, M. El-
1757 Balkimy, and M. Abou Donia. 2017. "Elevated Serum α-Synuclein Autoantibodies in
1758 Patients with Parkinson's Disease Relative to Alzheimer's Disease and Controls." *Front*
1759 *Neurol* 8:720. doi: 10.3389/fneur.2017.00720.

1760 Singh, N. N., and D. P. Ramji. 2008. "Protein kinase CK2, an important regulator of the
1761 inflammatory response?" *J Mol Med (Berl)* 86 (8):887-97. doi: 10.1007/s00109-008-
1762 0352-0.

1763 Singhrao, S. K., J. W. Neal, B. P. Morgan, and P. Gasque. 1999. "Increased
1764 complement biosynthesis by microglia and complement activation on neurons in
1765 Huntington's disease." *Exp Neurol* 159 (2):362-76. doi: 10.1006/exnr.1999.7170.

1766 Smith-Dijak, A. I., M. D. Sepers, and L. A. Raymond. 2019. "Alterations in synaptic
1767 function and plasticity in Huntington disease." *J Neurochem* 150 (4):346-365. doi:
1768 10.1111/jnc.14723.

1769 Sofroniew, M. V. 2009. "Molecular dissection of reactive astrogliosis and glial scar
1770 formation." *Trends Neurosci* 32 (12):638-47. doi: 10.1016/j.tins.2009.08.002.

1771 Southwell, A. L., A. Smith-Dijak, C. Kay, M. Sepers, E. B. Villanueva, M. P. Parsons, Y.
1772 Xie, L. Anderson, B. Felczak, S. Waltl, S. Ko, D. Cheung, L. Dal Cengio, R. Slama, E.
1773 Petoukhov, L. A. Raymond, and M. R. Hayden. 2016. "An enhanced Q175 knock-in

1774 mouse model of Huntington disease with higher mutant huntingtin levels and
1775 accelerated disease phenotypes." *Hum Mol Genet* 25 (17):3654-3675. doi:
1776 10.1093/hmg/ddw212.

1777 Steele-Perkins, G., C. Plachez, K. G. Butz, G. Yang, C. J. Bachurski, S. L. Kinsman, E.
1778 D. Litwack, L. J. Richards, and R. M. Gronostajski. 2005. "The transcription factor gene
1779 Nfib is essential for both lung maturation and brain development." *Mol Cell Biol* 25
1780 (2):685-98. doi: 10.1128/MCB.25.2.685-698.2005.

1781 Stout, J. C., R. Jones, I. Labuschagne, A. M. O'Regan, M. J. Say, E. M. Dumas, S.
1782 Queller, D. Justo, R. D. Santos, A. Coleman, E. P. Hart, A. Dürr, B. R. Leavitt, R. A.
1783 Roos, D. R. Langbehn, S. J. Tabrizi, and C. Frost. 2012. "Evaluation of longitudinal 12
1784 and 24 month cognitive outcomes in premanifest and early Huntington's disease." *J*
1785 *Neurol Neurosurg Psychiatry* 83 (7):687-94. doi: 10.1136/jnnp-2011-301940.

1786 Tai, Y. F., N. Pavese, A. Gerhard, S. J. Tabrizi, R. A. Barker, D. J. Brooks, and P.
1787 Piccini. 2007. "Imaging microglial activation in Huntington's disease." *Brain Res Bull* 72
1788 (2-3):148-51. doi: 10.1016/j.brainresbull.2006.10.029.

1789 Takahashi, M., L. W. Ko, J. Kulathingal, P. Jiang, D. Sevlever, and S. H. Yen. 2007.
1790 "Oxidative stress-induced phosphorylation, degradation and aggregation of alpha-
1791 synuclein are linked to upregulated CK2 and cathepsin D." *Eur J Neurosci* 26 (4):863-
1792 74. doi: 10.1111/j.1460-9568.2007.05736.x.

1793 Teravskis, P. J., A. Covelo, E. C. Miller, B. Singh, H. A. Martell-Martínez, M. A.
1794 Benneyworth, C. Gallardo, B. R. Oxnard, A. Araque, M. K. Lee, and D. Liao. 2018.

"A53T Mutant Alpha-Synuclein Induces Tau-Dependent Postsynaptic Impairment Independently of Neurodegenerative Changes." *J Neurosci* 38 (45):9754-9767. doi: 10.1523/JNEUROSCI.0344-18.2018.

Tkac, I., P. G. Henry, L. Zacharoff, M. Wedel, W. Gong, D. K. Deelchand, T. Li, and J. M. Dubinsky. 2012. "Homeostatic adaptations in brain energy metabolism in mouse models of Huntington disease." *J Cereb Blood Flow Metab* 32 (11):1977-88. doi: 10.1038/jcbfm.2012.104.

Tkác, I., Z. Starcuk, I. Y. Choi, and R. Gruetter. 1999. "In vivo 1H NMR spectroscopy of rat brain at 1 ms echo time." *Magn Reson Med* 41 (4):649-56. doi: 10.1002/(sici)1522-2594(199904)41:4<649::aid-mrm2>3.0.co;2-g.

Tomás-Zapico, C., M. Díez-Zaera, I. Ferrer, P. Gómez-Ramos, M. A. Morán, M. T. Miras-Portugal, M. Díaz-Hernández, and J. J. Lucas. 2012. "α-Synuclein accumulates in huntingtin inclusions but forms independent filaments and its deficiency attenuates early phenotype in a mouse model of Huntington's disease." *Hum Mol Genet* 21 (3):495-510. doi: 10.1093/hmg/ddr507.

Turner, M. D., B. Nedjai, T. Hurst, and D. J. Pennington. 2014. "Cytokines and chemokines: At the crossroads of cell signalling and inflammatory disease." *Biochim Biophys Acta* 1843 (11):2563-2582. doi: 10.1016/j.bbamcr.2014.05.014.

Vercauteren, F. G., G. Flores, W. Ma, J. G. Chabot, L. Geenen, S. Clerens, A. Fazel, J. J. Bergeron, L. K. Srivastava, L. Arckens, and R. Quirion. 2007. "An organelle proteomic

1815 method to study neurotransmission-related proteins, applied to a neurodevelopmental
1816 model of schizophrenia." *Proteomics* 7 (19):3569-79. doi: 10.1002/pmic.200700379.

1817 Vezzani, A., T. Ravizza, S. Balosso, and E. Aronica. 2008. "Glia as a source of
1818 cytokines: implications for neuronal excitability and survival." *Epilepsia* 49 Suppl 2:24-
1819 32. doi: 10.1111/j.1528-1167.2008.01490.x.

1820 Vezzoli, E., I. Caron, F. Talpo, D. Besusso, P. Conforti, E. Battaglia, E. Sogne, A.
1821 Falqui, L. Petricca, M. Verani, P. Martufi, A. Caricasole, A. Bresciani, O. Cecchetti, P.
1822 Rivetti di Val Cervo, G. Sancini, O. Riess, H. Nguyen, L. Seipold, P. Saftig, G. Biella, E.
1823 Cattaneo, and C. Zuccato. 2019. "Inhibiting pathologically active ADAM10 rescues
1824 synaptic and cognitive decline in Huntington's disease." *J Clin Invest* 129 (6):2390-
1825 2403. doi: 10.1172/JCI120616.

1826 Waxman, E. A., and B. I. Giasson. 2008. "Specificity and regulation of casein kinase-
1827 mediated phosphorylation of alpha-synuclein." *J Neuropathol Exp Neurol* 67 (5):402-16.
1828 doi: 10.1097/NEN.0b013e31816fc995.

1829 Waxman, E. A., and B. I. Giasson. 2011. "Characterization of kinases involved in the
1830 phosphorylation of aggregated α-synuclein." *J Neurosci Res* 89 (2):231-47. doi:
1831 10.1002/jnr.22537.

1832 Wood, T. E., J. Barry, Z. Yang, C. Cepeda, M. S. Levine, and M. Gray. 2019. "Mutant
1833 huntingtin reduction in astrocytes slows disease progression in the BACHD conditional
1834 Huntington's disease mouse model." *Hum Mol Genet* 28 (3):487-500. doi:
1835 10.1093/hmg/ddy363.

1836 Xu, X., P. A. Toselli, L. D. Russell, and D. C. Seldin. 1999. "Globozoospermia in mice
1837 lacking the casein kinase II alpha' catalytic subunit." *Nat.Genet.* 23 (1):118-121.

1838 Yamatani, H., T. Kawasaki, S. Mita, N. Inagaki, and T. Hirata. 2010. "Proteomics
1839 analysis of the temporal changes in axonal proteins during maturation." *Dev Neurobiol*
1840 70 (7):523-37. doi: 10.1002/dneu.20794.

1841 Zach, S., H. Bueler, B. Hengerer, and F. Gillardon. 2007. "Predominant neuritic
1842 pathology induced by viral overexpression of alpha-synuclein in cell culture." *Cell Mol*
1843 *Neurobiol* 27 (4):505-15. doi: 10.1007/s10571-007-9141-5.

1844 Zeron, M. M., O. Hansson, N. Chen, C. L. Wellington, B. R. Leavitt, P. Brundin, M. R.
1845 Hayden, and L. A. Raymond. 2002. "Increased sensitivity to N-methyl-D-aspartate
1846 receptor-mediated excitotoxicity in a mouse model of Huntington's disease." *Neuron* 33
1847 (6):849-60.

1848 Öz, G., E. Kittelson, D. Demirgöz, O. Rainwater, L. E. Eberly, H. T. Orr, and H. B. Clark.
1849 2015. "Assessing recovery from neurodegeneration in spinocerebellar ataxia 1:
1850 Comparison of in vivo magnetic resonance spectroscopy with motor testing, gene
1851 expression and histology." *Neurobiol Dis* 74:158-66. doi: 10.1016/j.nbd.2014.11.011.

1852

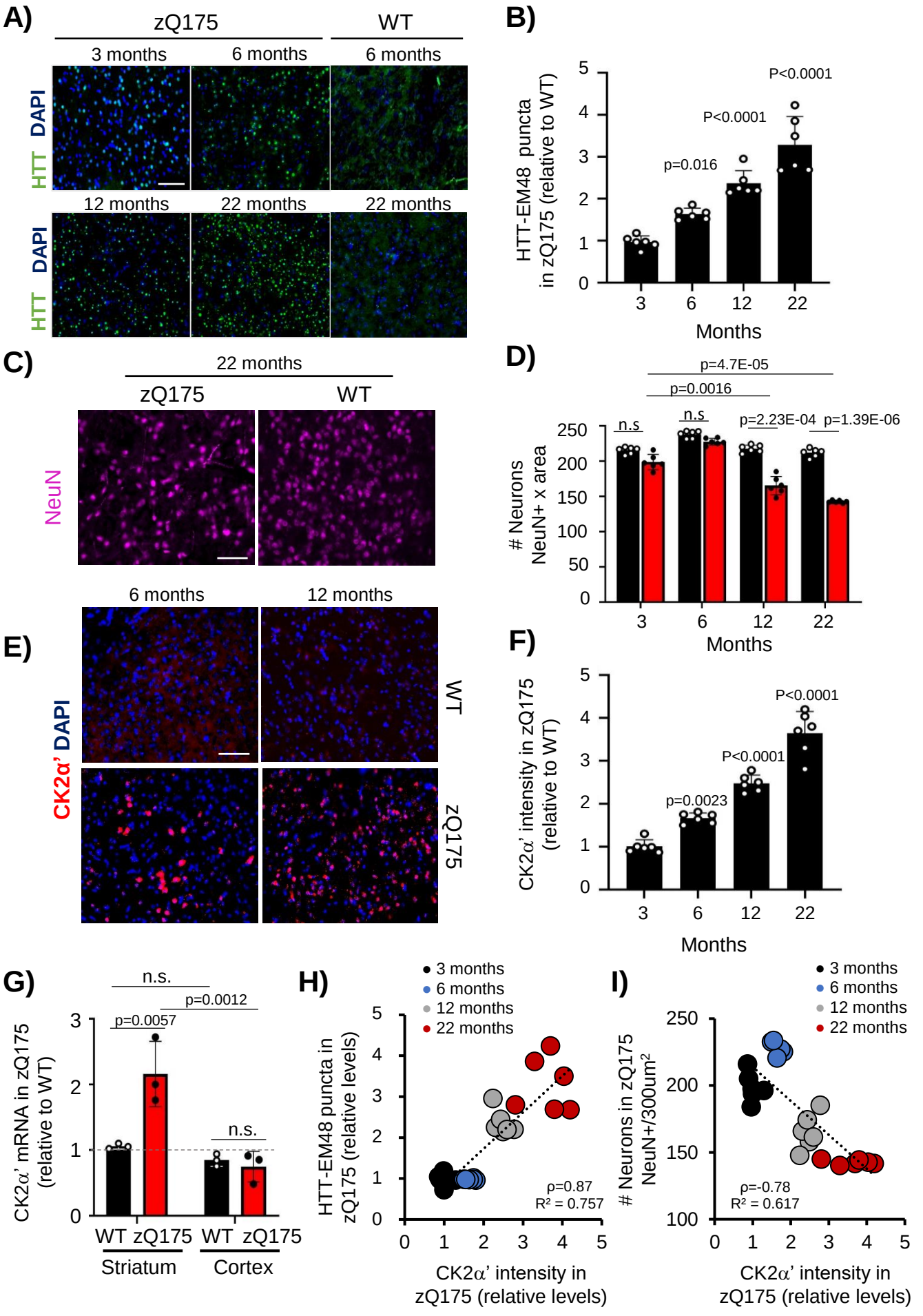


**Figure 1**

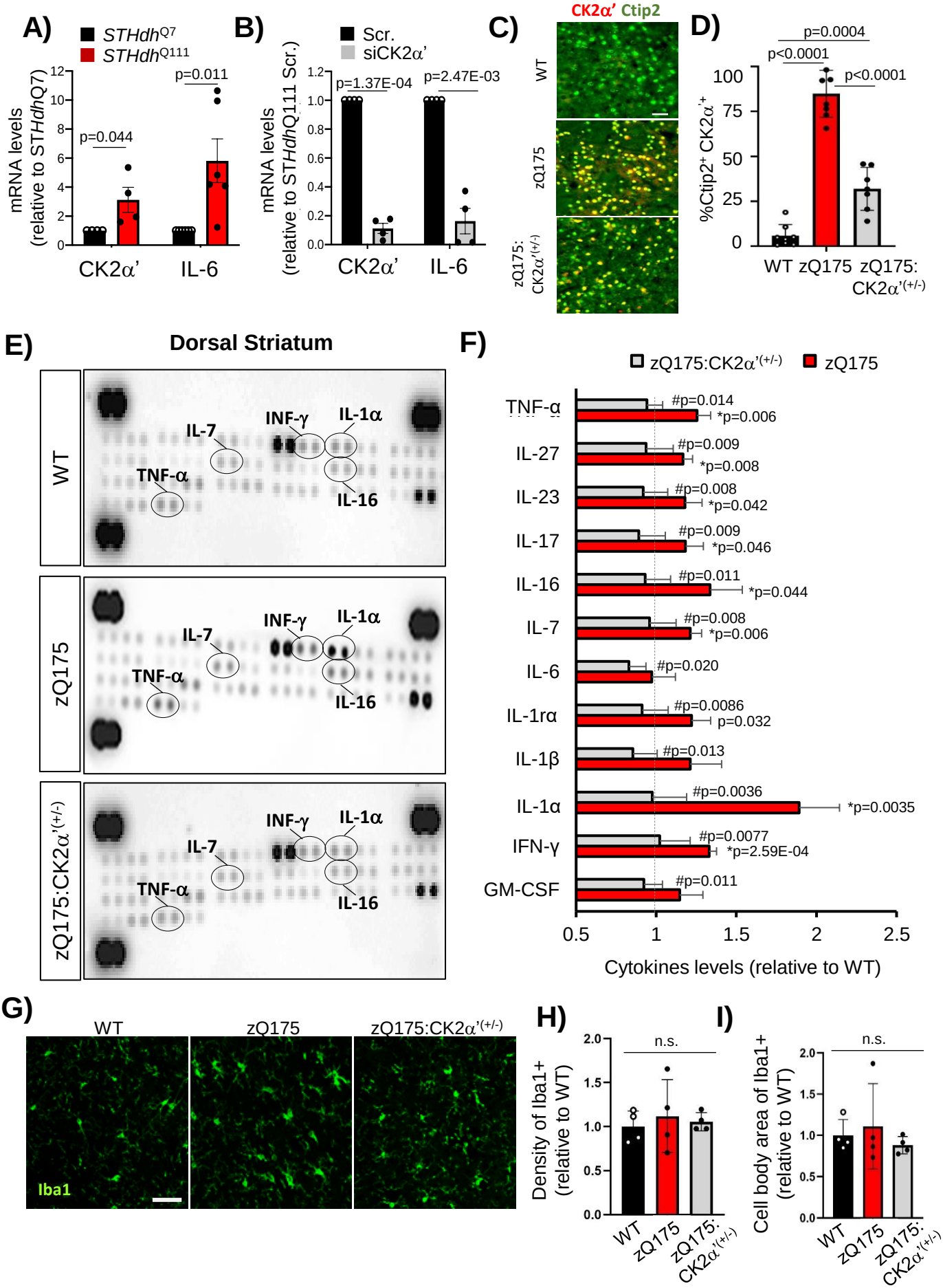


**Figure 2**

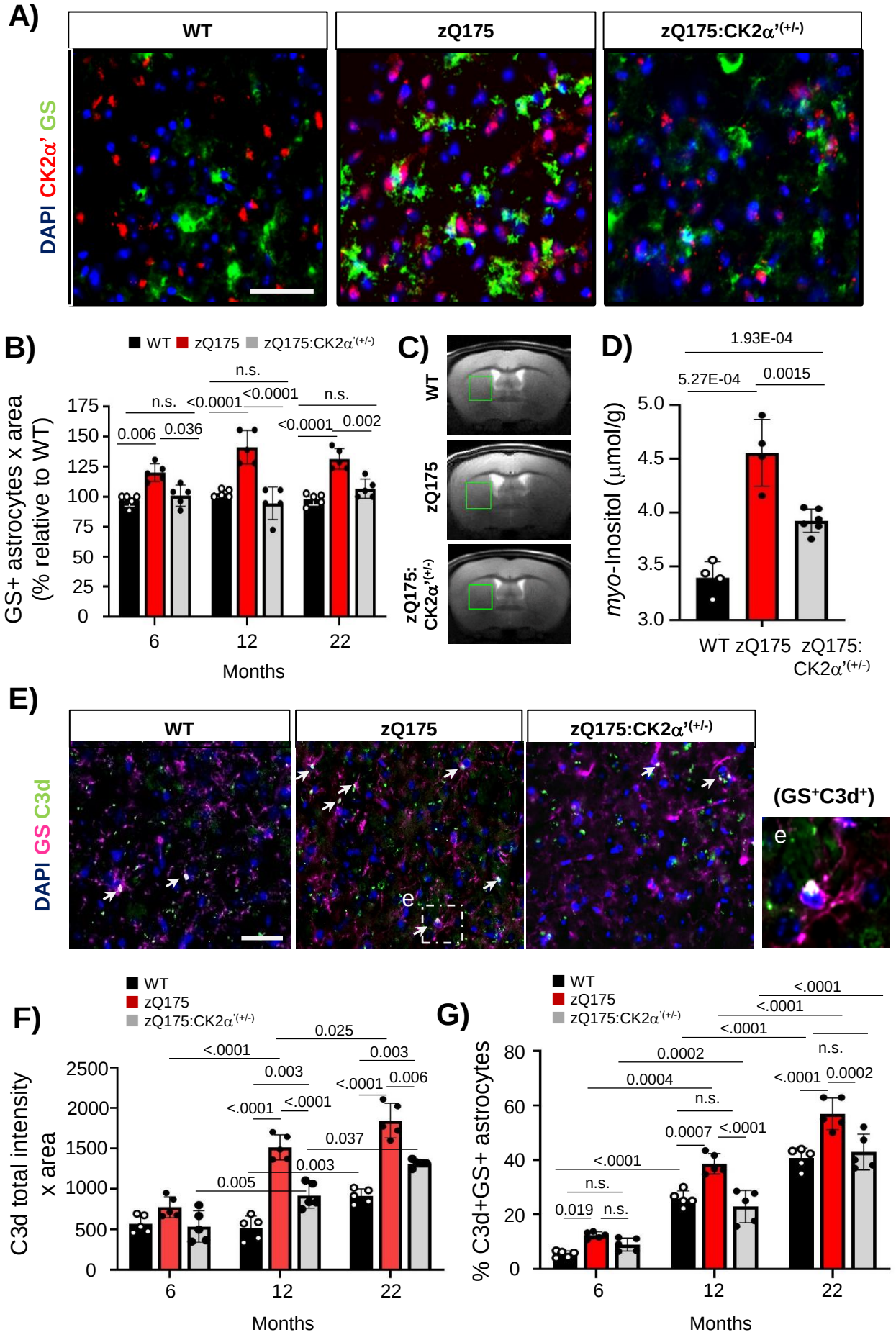


**Figure 3**

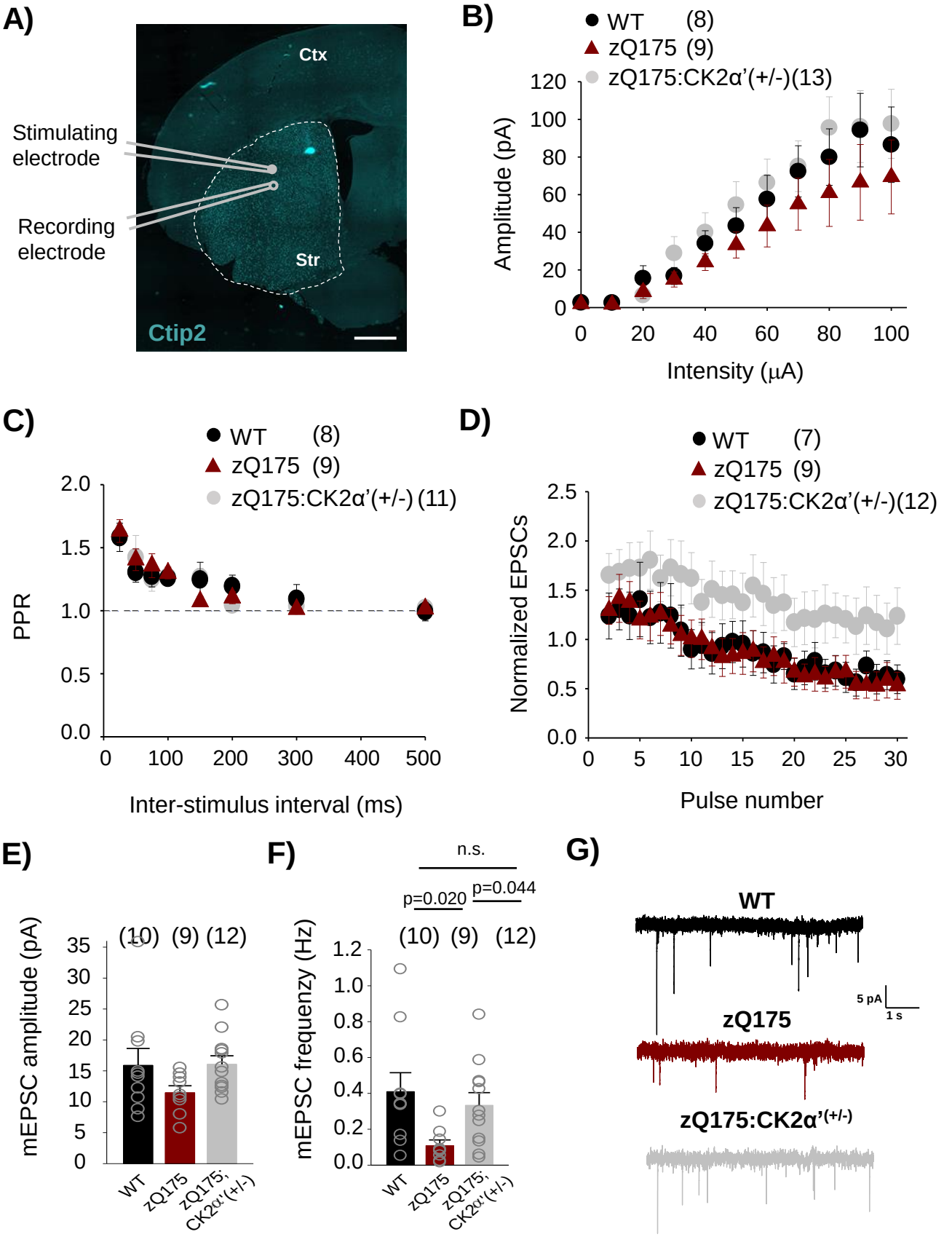


**Figure 4**

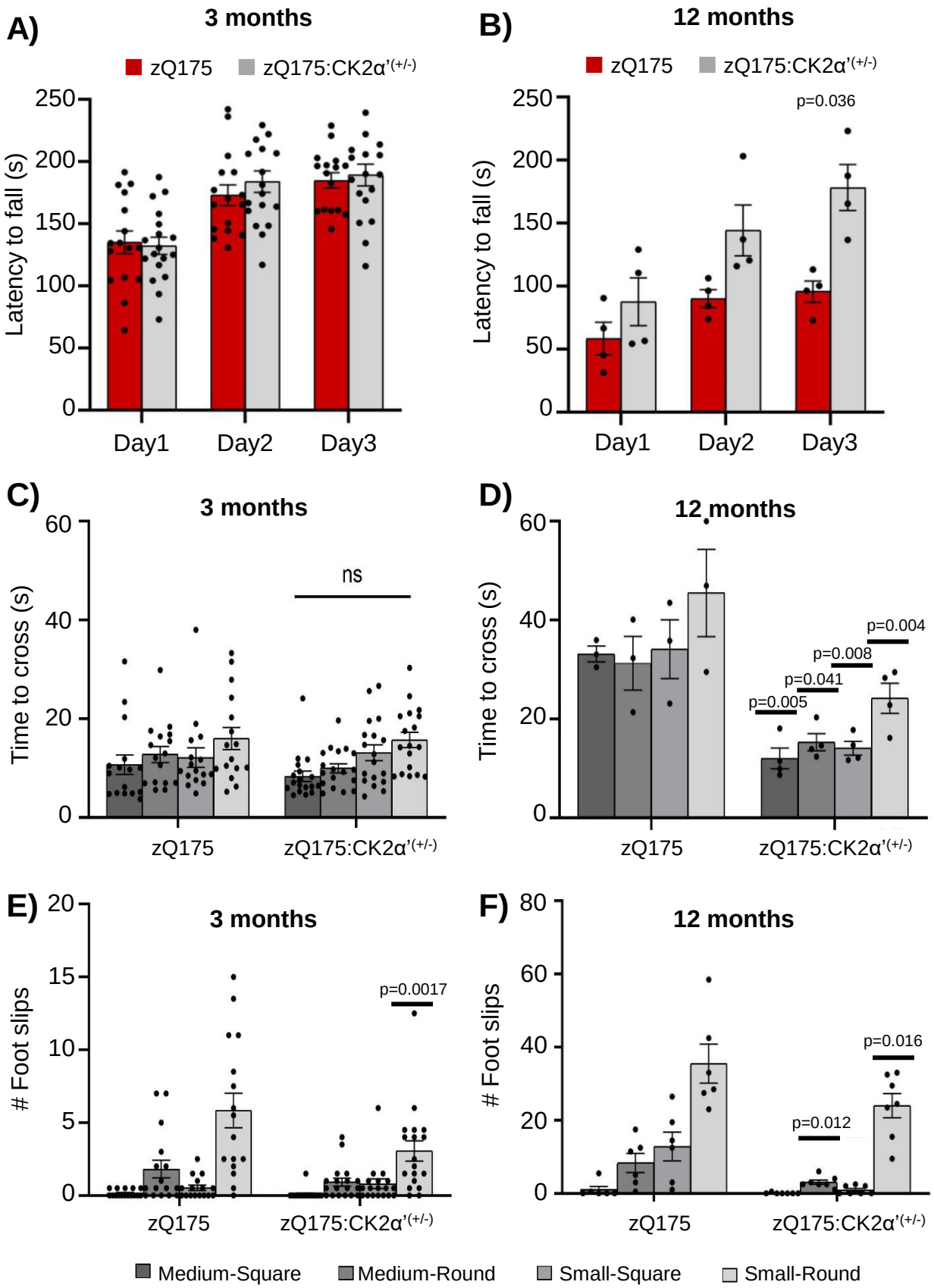


**Figure 5**

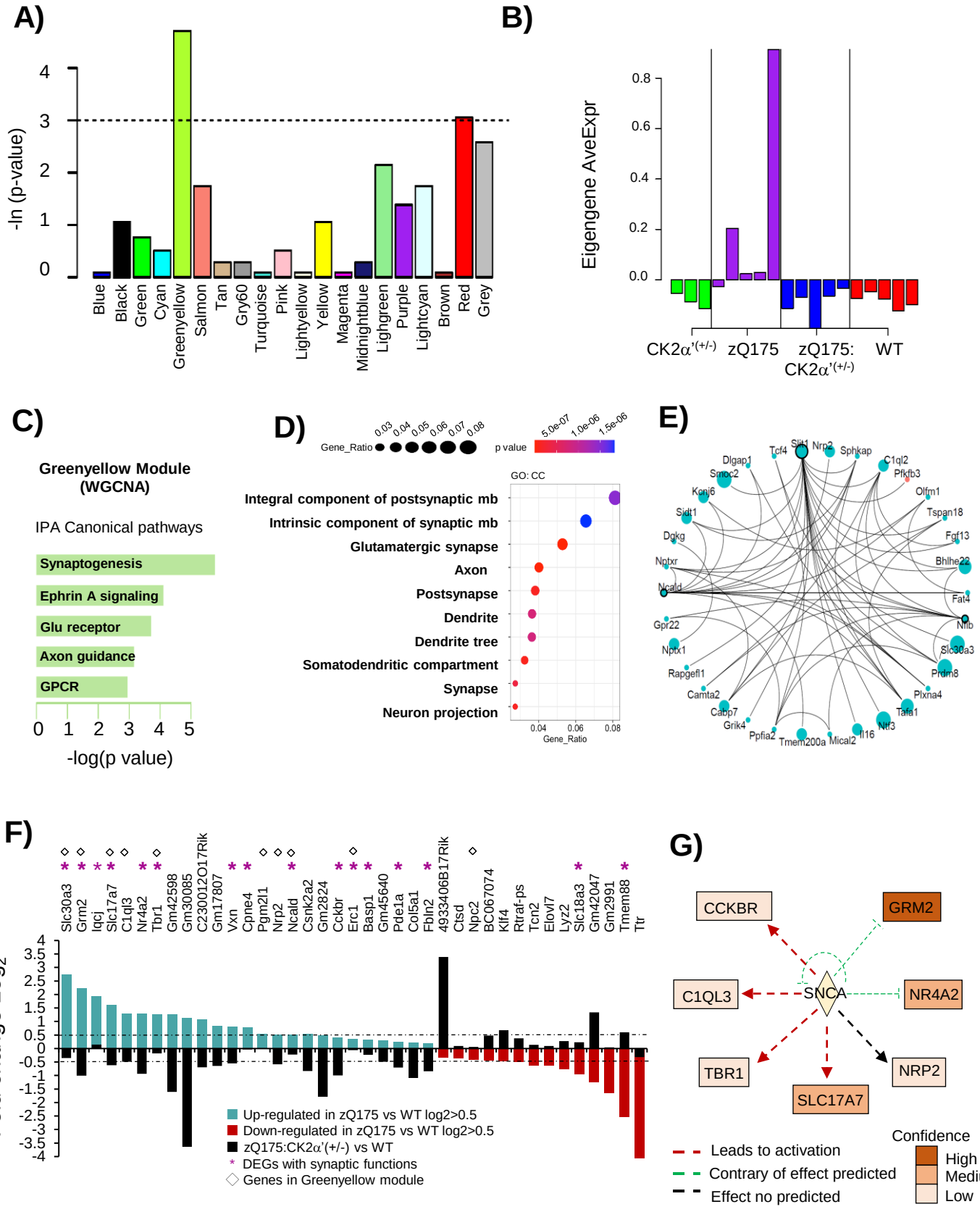


**Figure 6**

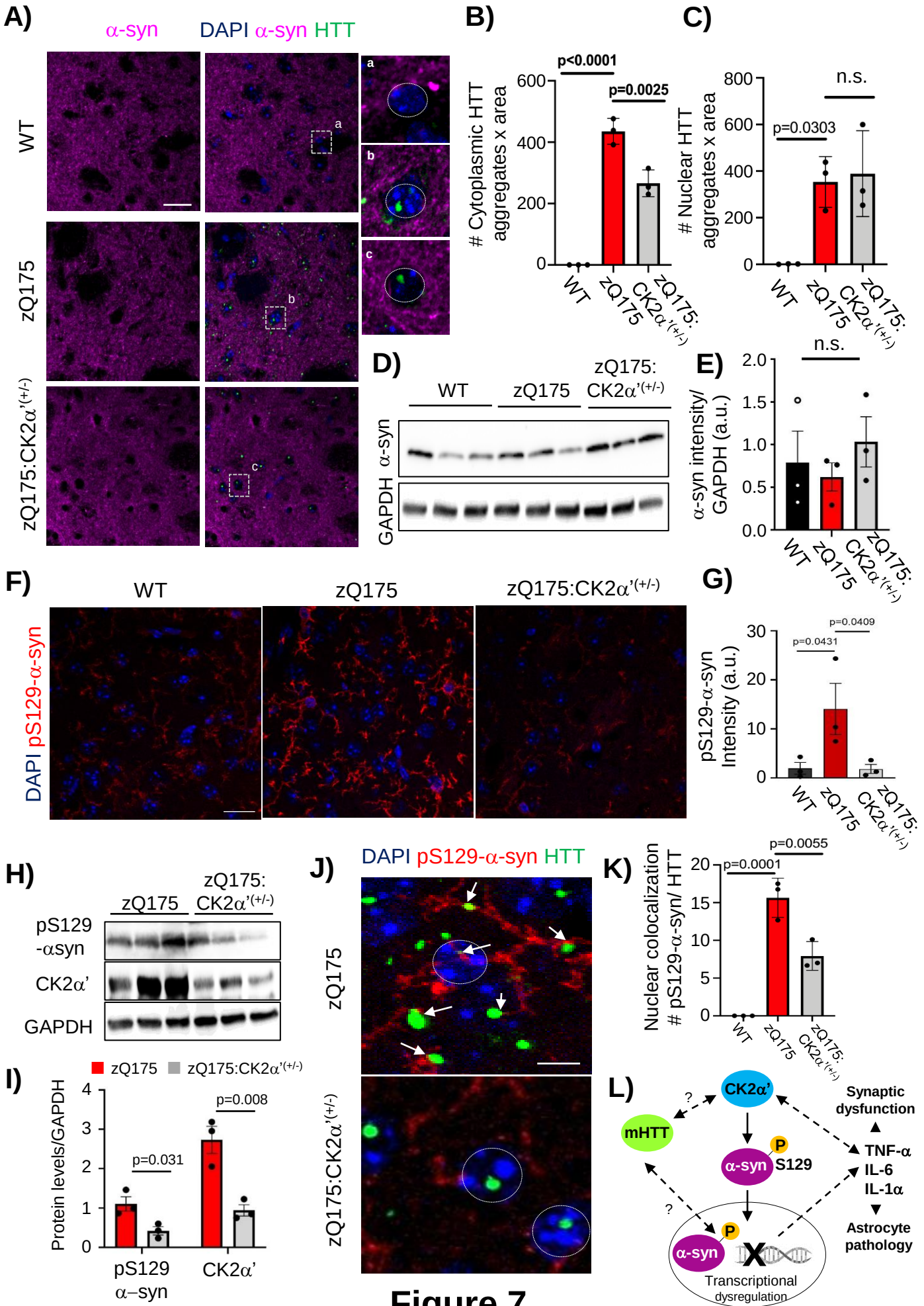


**Figure 7**